Contrib Mineral Petrol (1999) 135: 93–113

Michel Jaboyedoff · Michael A. Cosca

Dating incipient metamorphism using $^{40}Ar/^{39}Ar$ geochronology and XRD modeling: a case study from the Swiss Alps

Received: 26 June 1998 / Accepted: 16 November 1998

Abstract Six samples of a single carbonate-rich unit of the Swiss Préalpes, progressively metamorphosed from diagenesis to deep anchizone, yield $^{40}Ar/^{39}Ar$ spectra with variably developed staircase patterns, consistent with mixtures of detrital mica and neocrystallized mixed-layer illite/smectite. The lowest temperature heating steps for different size fractions (2–6 μm and 6–20 μm) converge to ~40 Ma providing an imprecise, maximum age of regional metamorphism. A method is described for distinguishing and quantifying the amount of pre-existing detrital mica versus neoformed illite layer in the illite/smectite formed during Tertiary Alpine metamorphism by comparison of X-ray diffraction patterns with Newmod© simulations. In the least metamorphosed samples the illite/smectite contains ~65% neoformed illite, and this illite accounts for approximately 17% of all dioctahedral phyllosilicate minerals in the rock (e.g., detrital mica and illite/smectite). In contrast, the illite/smectite from the more strongly metamorphosed samples contains >97% neoformed illite, which accounts for ~70% to >90% of all dioctahedral phyllosilicate minerals. Phyllosilicate morphologies viewed by scanning electron microscopy are consistent with these estimates. A process of dissolution/reprecipitation is inferred as a mechanism for the growth of the neoformed phyllosilicates. A plot of neoformed illite content versus $^{40}Ar/^{39}Ar$ total fusion age yields a near-linear curve with an extrapolated age of 27 Ma for 100% neoformed dioctahedral phyllosilicates. This age is interpreted as the time of incipient metamorphism and is consistent with independent biostratigraphic constraints. Model $^{40}Ar/^{39}Ar$ age spectra constructed with the XRD simulation results correspond well to the experimental data and illustrate the changes in degassing properties of progressively metamorphosed mixtures of detrital mica and neoformed illite.

M. Jaboyedoff · M.A. Cosca (✉)
Institut de Minéralogie, Université de Lausanne,
CH-1015 Lausanne, Switzerland
E-mail: mcosca@imp.unil.ch

Editorial responsibility: J. Hoefs

Introduction

Isotopic dating of phyllosilicates in very low grade metamorphic rocks by K/Ar or $^{40}Ar/^{39}Ar$ methods is strongly dependent on the ratio of detrital mica versus authigenic (neoformed) mixed-layer illite/smectite present in the separated size fraction (see review in Clauer and Chaudhuri 1995). With increasing depth in sedimentary basins (burial metamorphism) K/Ar ages of phyllosilicate fractions decrease together with a corresponding increase in illite content within the mixed-layer illite/smectite (e.g., Perry 1974; Aronson and Hower 1976; Glasmann et al. 1989). Furlan et al. (1996) have also shown that the magnitude of the apparent age decrease is lithology dependent and is greater in sandstones than in shales. Very low grade regional metamorphic rocks represent a natural extension of metamorphism occurring in sedimentary basins, but the size of neoformed phyllosilicates is generally larger. With increasing illite crystallinity the apparent K/Ar and $^{40}Ar/^{39}Ar$ ages of phyllosilicate fractions generally become younger and the smallest size fraction is generally the youngest (e.g., Hunziker et al. 1986; Reuter 1987; Reuter and Dallmeyer 1989; Brockamp et al. 1994).

For the special case where no detrital mica or illite is present, such as in pure sandstones or bentonites, the effects of diagenesis producing illite/smectite can result in increasingly older apparent ages with depth (e.g., Hamilton et al. 1989; Matthews et al. 1994; Velde and Renac 1996). The geological significance of such ages is strongly dependent on the duration of the transformation(s) and the continuous production of illite with depth (Clauer et al. 1997). In a porous medium like sandstone or hydrothermal systems, illite crystallization is facilitated and can be extremely rapid (Barnes et al. 1992; Matthews et al. 1994; Bonhomme et al. 1995; Clauer et al. 1997).

More complicated results have been observed in shales of the North Sea (Glassman et al. 1989), where the apparent ages of the >1 μm size fractions decrease with depth, yet remain older than the stratigraphic age (Aronson and Hower 1976; Clauer et al. 1997). In this case neoformed illite often seems to form overgrowths on nuclei of detrital grains, while smaller size fractions (<0.1 μm) yielded apparent ages younger than the stratigraphic age. In a study of Jurassic sandstone off the coast of Alabama, Thomas et al. (1993) report $^{40}Ar/^{39}Ar$ laser fusion ages of pure, authigenic illite with no detrital mica and conclude that illite was formed during a period of 80 Ma (120–40 Ma) by stylolitization of K-feldspar.

Theoretically, no detrital micas should occur in the fine size fractions extracted from bentonites, and should yield ages dependent entirely on the production of neoformed illite layers (Altaner 1989). Furthermore, in some diagenetic bentonites and shales Clauer et al. (1997) report that the thinnest fundamental particles have ages equivalent to, or older than, thicker ones, indicating illite growth around previously precipitated illite.

Mossmann et al. (1992), Pevear (1992) and Grathoff and Moore (1996) combined K/Ar and X-ray diffraction data from different size fractions of illite to distinguish between detrital and neoformed (diagenetic) illite or between several generations of authigenic illite. These authors suggested that if the detrital and neoformed illite exhibit a nearly linear dependence when plotted on a diagram of age versus % detrital illite, the curve could be extrapolated to 0% detrital mica to yield an age of illitization. The linearity is an acceptable approximation for curves of a two component mixture with end-member ages differing by less than 500 Ma. Pevear (1992) obtained an illite age consistent with a calculated age for its formation. In addition, artificial mixtures of mica and illite/smectite yielded staircase $^{40}Ar/^{39}Ar$ spectra, and when combined with such XRD modeling gave extrapolated results for the end-member ages in reasonable agreement with their known ages (Onstott et al. 1997).

Staircase $^{40}Ar/^{39}Ar$ spectra have been observed in low- and high-grade regional metamorphic rocks and have been interpreted as mixtures of different generations of mica and/or illites (e.g., Wijbrans and McDougall 1986; Kirschner et al. 1996). Because argon appears to be retained in the mineral lattice of micas and illite to much higher temperatures than previously thought (e.g., Hames and Bowring 1994; Kirschner et al. 1996), it should be possible in certain cases to determine the end-member ages of two component mixtures in low-grade regional metamorphic rocks. In this paper we combine progressively developed staircase $^{40}Ar/^{39}Ar$ spectra, interpreted as mixtures of detrital Permo-Carboniferous and neoformed Tertiary phyllosilicates, with modeled X-ray diffraction data to identify the age of the youngest end-member of the mixtures (neoformed illite), which records the timing of low-grade, regional metamorphism.

Geology

The Préalpes of Switzerland (Fig. 1) comprise a sequence of nappes mainly consisting of carbonate and flysch of Triassic to Eocene age (Baud and Septfontaine 1980; Trümpy 1980; Mosar 1989, 1991). The Préalpes Médianes represents one of the major units of the Préalpes, which was derived from carbonate platform rocks of the Briançonnais and sub-Briançonnais domain (Baud and Septfontaine 1980; Trümpy 1980; Stampfli et al. 1998). The youngest sediments of the Préalpes Médianes are flysch of middle Eocene age (~47 to ~40 Ma, Caron et al. 1989). Stratigraphically below the flysch is the Couches Rouges, a thin marly limestone of late Cretaceous to early Tertiary (90–47 Ma) age (Guillaume 1986).

The emplacement history of the Préalpes Médianes nappe sequence is described elsewhere (Mosar 1989, 1991; Sartori 1990; Epard and Escher 1996; Escher et al. 1997). The tectonic burial of the Préalpes Médianes was due to overthrusting from the southeast, as these cover rocks were detached from their basement. The basement and equivalent cover series underwent greenschist facies metamorphism around 38–34 Ma (Escher et al. 1997; Markley et al. 1998). Thrusting of the Préalpes Médianes onto the Molasse occurred sometime after upper Oligocene, as indicated by the presence of overthrusted sediments of this age (~25 Ma, Badoux 1996; Burkhard and Sommaruga in press).

In the Préalpes Médianes, incipient metamorphism increases from diagenesis to deep anchizone, as reflected by changing mineral parageneses and illite crystallinity, with a general increase from northwest to southeast (Baud 1987; Mosar 1988; Jaboyedoff and Thélin 1996). In the Couches Rouges, this progressive metamorphism is expressed by the replacement of stylolites by a slaty cleavage with increasing metamorphism.

Methods

Samples

All samples come from progressively metamorphosed (diagenesis to anchizone) marly limestones of the Couches Rouges, which were collected at different locations within the Préalpes Médianes (Fig. 1). The calcite content for all samples is 80–90 wt% (estimated by weight loss upon dissolution of the carbonates, Jaboyedoff and Thélin 1996), and the remaining constituents are 10–15% clay minerals, ~4% quartz, and ~1% albite; K-feldspar is absent or occurs only in very small amounts.

Different grain size fractions were separated from limestone and marly limestone of the Couches Rouges after crushing to about 2 mm and dissolution of the carbonates in 2 M HCl followed by washing in distilled water (pH ~5.6). No significant effect on K/Ar ages has been observed from acid dissolution experiments involving phyllosilicate minerals (Clauer et al. 1993). The 2–6 μm and 6–20 μm size fractions were isolated by centrifugation to remove the <2 μm fractions and the residue was separated by gravity sedimentation using distilled water with a constant pH of approximately 7.5 maintained by adding a NaOH solution. In order to eliminate potential Ca contamination in the samples, all size fractions were saturated with Mg^{2+} using a 2 M $MgCl_2$ solution for at least 24 hours, during which time the solution was changed twice. After the $MgCl_2$ treatment the samples were thoroughly washed with distilled water. One aliquot of sample 345 (1345) was also prepared with no Mg^{2+} saturation.

XRD

For each size fraction of every sample one oriented and one disoriented powder specimen was prepared for X-ray diffraction (XRD) analysis. The oriented specimen was prepared by sedimentation of more than 2.5 mg/cm^2 on a glass slide. The XRD data were collected with a 185 mm radius Rigaku horizontal

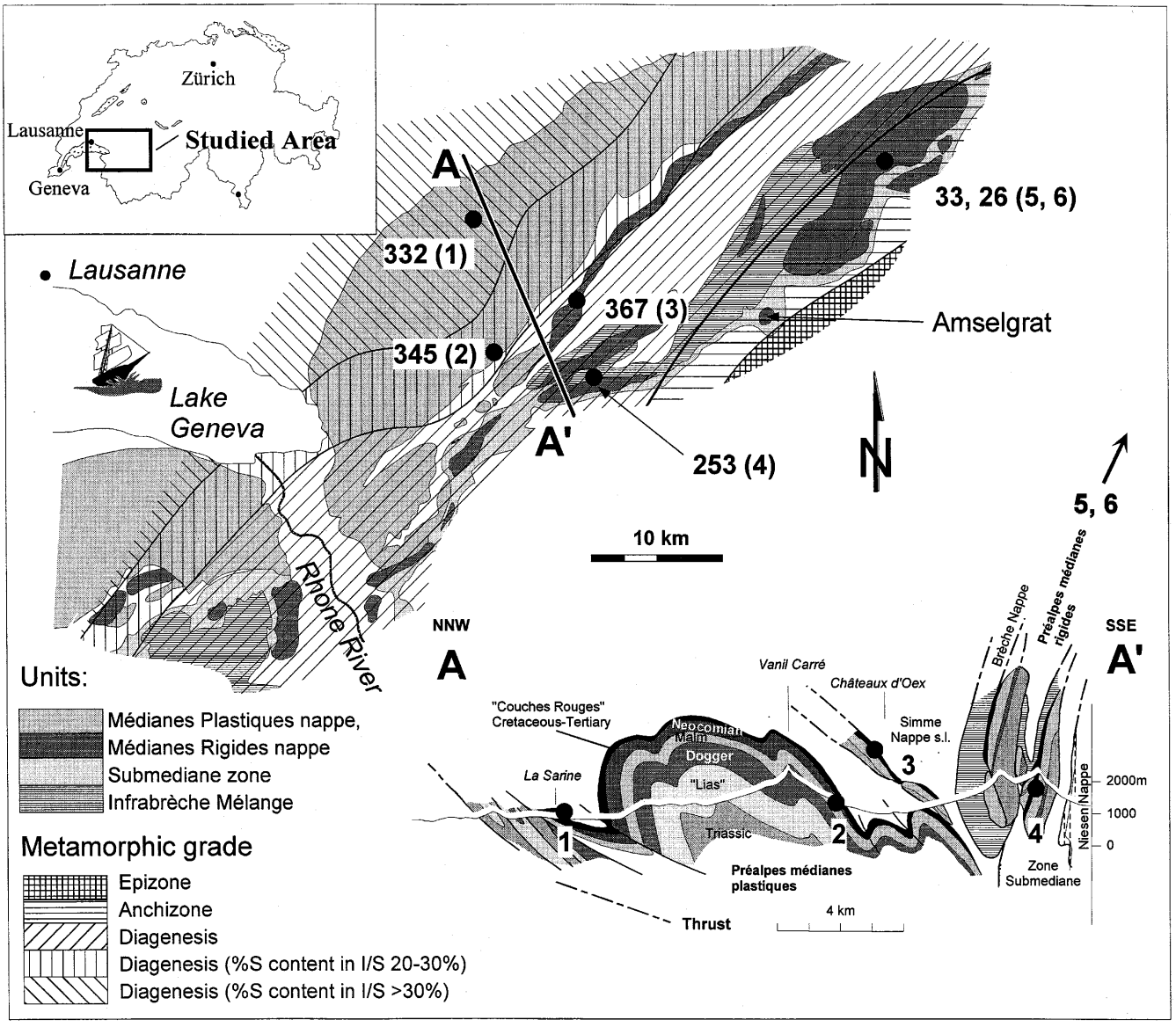

Fig. 1 Schematic tectonic and metamorphic map of the Swiss Préalpes. The position of samples is indicated and *numbers in parentheses* make reference to the corresponding sample number used in Jaboyedoff and Thélin (1996)

powder diffractometer (Geigerflex) equipped with a rotating Cu anode (Cu Kα radiation, nickel filter, 0.5° divergent and scatter slits, 0.15 mm receiving slit and 2 Soller slits of 5°). All samples were analyzed with the same conditions of 40 kV and 30 mA scanned from 2–50° 2θ in 1 second steps of 0.01°. Five XRD diffractograms were obtained for each size fraction, which include air-dried (AD) and ethylene glycol (EG) saturations for both preparation types and the oriented sample again after heating at 350 °C for 5 hours. The 060 reflections were determined using the disoriented 2–6 μm fractions using 2° divergent and scatter slits, and a 0.3 mm receiving slit.

In order to interpret the XRD data, we have made the assumption that in the clay fractions the mixed-layer minerals contain no more than two components. This hypothesis is simplistic as shown by Drits et al. (1997) and Shau et al. (1990), but sufficient for our purpose. In this study the dioctahedral mica-like clay mineral illite occurring in the mixed-layer illite/smectite (Meunier and Velde 1989; Srodon et al. 1992) is considered as neoformed. For the Newmod© simulations the inherited micas have been simulated by pure dioctahedral mica. This distinction is slightly different from that of Jaboyedoff and Thélin (1996) but is not critical when comparing the results. In order to determine the percentage of neoformed illite layer in the samples the XRD diffractograms of the oriented slides were compared to the sum of modeled XRD diffractograms for pure dioctahedral mica (detrital) and mixed-layer dioctahedral mica (neoformed) – dioctahedral smectite (Pevear and Schuette 1993). The pure chlorite and pure smectite have not been simulated, because simulations of such low concentrations have little effect on the shape of the background and do not interfere with the mica or illite/smectite diffractograms. The program Newmod© (Reynolds 1985; Reynolds and Reynolds 1996) was used for the simulations and the best agreement between the measured and modeled diffractograms was determined visually. Modeling was only performed for the 2–6 μm size fraction. Oriented ethylene glycol preparations were used because the signals are similar but more intense than disoriented preparations. Moreover, the stability of the sample is improved when the two water layers of the mixed-layer illite/smectite structure are replaced by ethylene glycol. In our surroundings the relative humidity is usually 50–70% but in the laboratory it is generally around 45–50%. In non-glycolated samples, used as trials for the simulations, water loss from the two water layers of the illite/smectite structure can directly be observed

with time as peak positions migrate to the one water position and the Scherrer width of the 10 Å peak diminishes.

Using the hypothesis of two component mixed-layers, the main criterion for accepting a modeled XRD diffractogram for a given sample is that, using the proportions of smectite in mixed-layer illite/smectite and their overall abundance determined from simulation of the ethylene glycol diffractograms, good agreement must be observed between the measured and simulated diffractograms for both the air-dried and heated preparations. This must be performed considering that some 1 water smectite interlayer can occur in the air-dried preparations and some strain in the heated preparations can affect the shape of the measured diffractograms and are therefore slightly different than the simulations.

The simulations were performed by varying the number of layers, the fraction of dioctahedral mica in the mixed-layer illite/smectite and the Reichweite using most of the default Newmod© parameters (d-spacing dioctahedral mica = 9.98–9.94 Å or 9.95 Å for the most metamorphic samples 33 and 26; dioctahedral smectite-2 glycol layers = 16.9 Å; dioctahedral smectite-2 water layers = 15 Å; dioctahedral smectite-1 water layer = 12.5 Å) with the following additional parameters: 0.5° divergent slit; CuKα radiation; 18.5 cm goniometer radius, sample length 2.8 cm; two Soller slits of 5°; Mg exchange cation. A formula unit was defined as containing 0.9 K and 0.1 Fe per $(Si,Al)_4O_{10}$ for dioctahedral mica and 0.1 Fe per $(Si,Al)_4O_{10}$ for dioctahedral smectite. Because only CuKα radiation was used for Newmod© simulations, the position of the 3.33 Å basal reflection is slightly shifted from its true position and for this reason it is not displayed.

The weight of dioctahedral illite in the illite/smectite was calculated taking into account the difference in molar weight between dioctahedral smectite and dioctahedral illite. The molar weight for illite/smectite ($M_{I/S}$) is given by:

$$M_{I/S} = \frac{\%I \times M_I + (1 - \%I) \times M_S}{100} \quad (1)$$

where $\%I$ is percentage of dioctahedral illite in the mixed layer, M_I is the molar weight of illite and M_S is the molar weight of smectite. For a given sample containing illite/smectite the weight percent of dioctahedral illite in the mixed layer can be determined by:

$$\text{wt}\% = \frac{\%I \times M_I}{100 \times M_{I/S}} \times w_{I/S} \quad (2)$$

where $w_{I/S}$ is the weight of the mixed-layer illite/smectite in the sample. In our study the physical parameters are given by the following:

Dioctahedral mica	397	gr/mol
Dioctahedral smectite-2glycol layers	493	gr/mol
Dioctahedral smectite-2water layers	420	gr/mol
Dioctahedral smectite-1water layer	406	gr/mol

$^{40}Ar/^{39}Ar$ measurements

The 2–6 μm and 6–20 μm size fractions for each sample together with standards were packaged in tin foil and irradiated for 20 MWh in the central thimble position of the TRIGA reactor in Denver, USA (Dalrymple et al. 1981). The samples were then placed in a high vacuum extraction line and incrementally heated using a double-vacuum resistance furnace. The noble gases were purified by exposure to a cryogenic trap and Zr/Al/Ti getters, and the argon isotopic compositions were determined by static mode analysis using a Mass Analyzer Products 215–50 mass spectrometer. Correction for the neutron flux was determined with an intralaboratory precision of 0.5% using the standards MMHB-1, assuming an age of 520.4 Ma (Samson and Alexander 1987) and HDBI with an age of 24.21 Ma (Hess and Lippolt 1994). Ages were determined from the raw data after correcting for blanks, mass discrimination, nucleogenic decay and interference. A complete description of the analytical procedures is given in Cosca et al. (1998).

Results

Dioctahedral mica and illite/smectite are the essential components of the non-carbonate minerals (Fig. 2). Chlorite occurs in samples 33, 253, 345 and 332 with some swelling layers in the metamorphic samples of lowest grade. Kaolinite can be present in very small quantities. Sample 332 is the least metamorphosed sample, containing 65% dioctahedral illite in illite/smectite, consistent with diagenesis and is equivalent to a burial depth of 3000–4000 m (Pollastro 1993). Samples 345, 367 and 253, respectively, show evidence of a progressive increase in the degree of metamorphism. Samples 26 and 33 are consistent with metamorphic conditions of deep anchizone. The "illite crystallinity" of the < 2 μm fractions is about 0.30° Δ2θ CuKα for samples 26 and 33 and 0.50° Δ2θ CuKα for sample 253, assuming anchizone limits of 0.25 and 0.42° Δ2θ CuKα (Jaboyedoff and Thélin 1996). Illite crystallinity is not applicable to the other samples because of their elevated smectite content in the mixed-layer illite/smectite.

Accurate estimation of mica polytypes is difficult for all samples because of weak reflections perhaps related to structure degradation during transport, insufficient disorientation in the powder preparations and/or the occurrence of albite. However, all samples show reflections consistent with $2M_1$ polytypes and only a few 1M reflections were observed for samples 332, 345 and 367. Decomposition techniques failed to resolve compositionally distinct populations that could be indicated from the 060 and 331 reflections. The d-spacing of the 060 reflection changes slightly with increasing metamorphism, ranging from 1.502 to 1.507 Å, indicating a more phengitic component.

$^{40}Ar/^{39}Ar$ geochronology

The $^{40}Ar/^{39}Ar$ data are given in Table 1 and presented as age spectrum diagrams in Fig. 3. The $^{40}Ar/^{39}Ar$ spectra for the 2–6 μm and the 6–20 μm size fractions have nearly identical staircase shapes (Fig. 3). With progressive metamorphism the shape of the $^{40}Ar/^{39}Ar$ spectra change from convex for the diagenetic samples to concave for the anchizonal samples with a corresponding decrease in their integrated $^{40}Ar/^{39}Ar$ total fusion ages. For each sample the low temperature heating steps for both size fractions yield apparent ages of 50–100 Ma, which are equal to or older than the stratigraphic age of these rocks. However, excluding the first steps from some samples the low temperature steps of all samples converge to a value of about 40 Ma. The increasingly older ages observed in the high temperature heating steps are oldest for the least metamorphic samples. For the least metamorphosed sample (332), a flat part of the $^{40}Ar/^{39}Ar$ spectrum corresponding to the high temperature heating steps yields an age of approximately 330 Ma for the 2–6 μm fraction and approximately

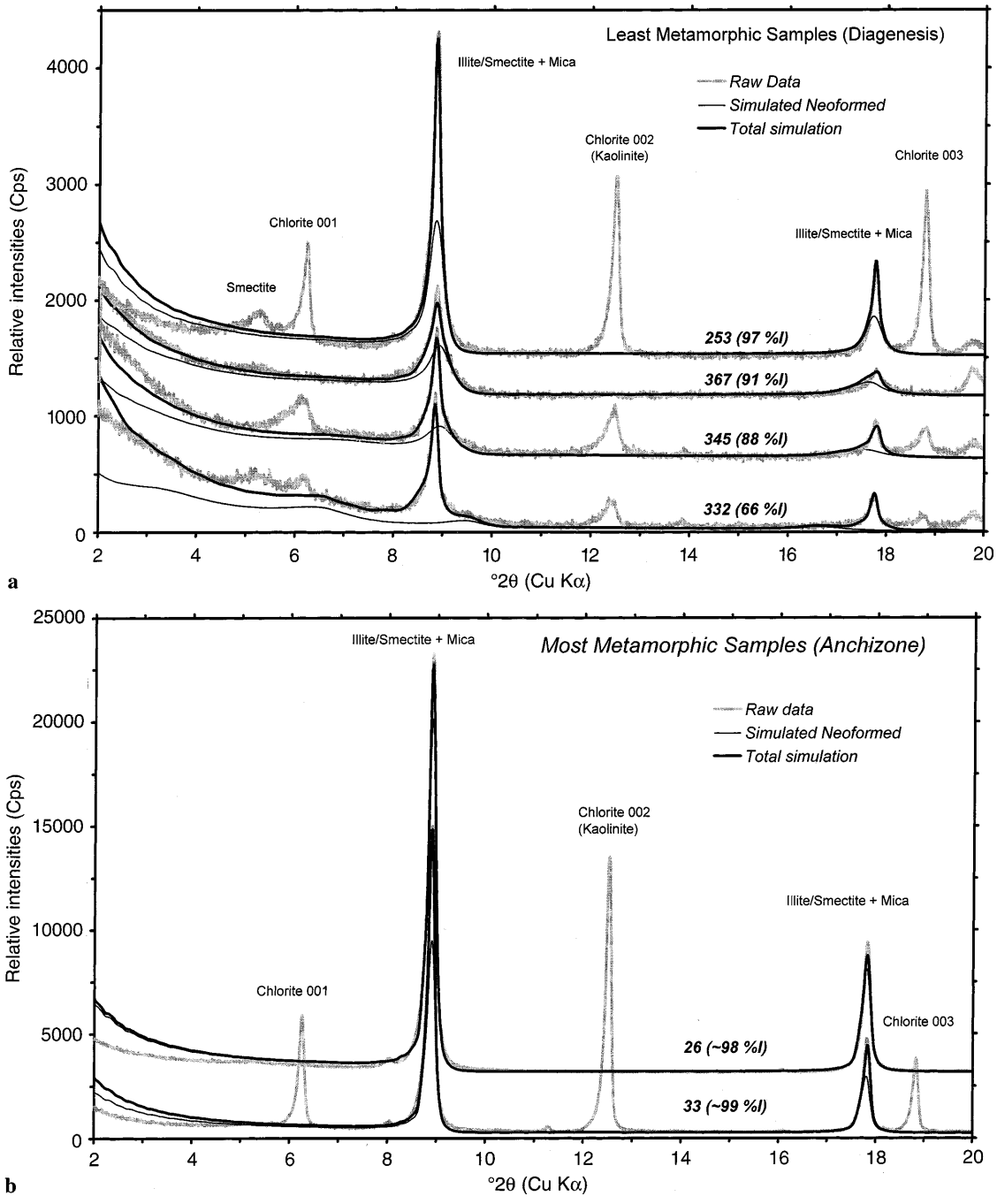

Fig. 2 **a** X-ray diffractograms and simulated XRD patterns for the least metamorphic (diagenetic) samples. The *numbers in parentheses* indicate the percentage of neoformed illite layer in the mixed-layer illite/smectite (Table 2). **b** X-ray diffractograms and simulated XRD patterns for the two most metamorphic (anchizone) samples. The *numbers in parentheses* indicate the percentage of neoformed illite layer in the mixed-layer illite/smectite, however the sharpness of the 10 Å peak prohibits a precise distinction between neoformed and detrital components (Table 2). The small peaks correspond to CuKβ peaks (a Ni filter is insufficient when intensities are high)

300 Ma for the 6–20 μm size fractions. The older age for the smaller size fraction, together with the shape of the $^{40}Ar/^{39}Ar$ spectrum could indicate some ^{39}Ar recoil. However, in other investigations using separates of 2–6 μm size the $^{40}Ar/^{39}Ar$ total fusion ages overlap with K-Ar ages, suggesting only minor argon loss due to recoil (e.g., Cosca et al. 1992). Recent work has shown that even in clay minerals of smaller grain sizes at equivalent metamorphic grades and composition the amount of ^{39}Ar loss due to recoil is about 5% (Dong et al. 1997; Onstott et al. 1997), thus indicating that recoiled ^{39}Ar is probably redistributed within the mineral and effectively scavenged in such materials, but further work is necessary to document this phenomenon.

The degassing of argon from a sample during laboratory heating is considered here to be dependent on the

Table 1 Analytical data for $^{40}Ar/^{39}Ar$ step heating experiments on white mica concentrates. All isotope data corrected for blanks, radioactive decay, interfering isotopes of argon and mass discrimination. K/Ca calculated from the $^{40}Ar/^{37}Ar$ ratio

T (°C)	^{40}Ar $\times 10^{-14}$moles	^{39}Ar $\times 10^{-14}$ moles	^{38}Ar $\times 10^{-14}$ moles	^{37}Ar $\times 10^{-14}$ moles	^{36}Ar $\times 10^{-14}$ moles	$^{40}Ar^{a}/^{39}Ar$	$\%^{39}Ar_K$	$\%^{40}Ar^{a}$	K/Ca	Age $\pm 2\sigma$
332 (2–6 μm) J = 0.004965 ± 0.5%; wt = 4.58 mg										
500	135.56 ± 4.28	4.856 ± 0.105	0.050 ± 0.002	3.795 ± 0.122	0.2279 ± 0.0007	14.11	5.77	50.50	0.65	122.2 ± 6.1
525	21.69 ± 0.31	1.006 ± 0.011	0.022 ± 0.000	3.898 ± 0.087	0.0353 ± 0.0002	11.51	1.20	53.30	0.13	100.3 ± 3.0
550	25.99 ± 0.22	1.127 ± 0.009	0.034 ± 0.000	6.483 ± 0.068	0.0329 ± 0.0003	14.93	1.34	64.50	0.09	129.0 ± 2.4
575	30.02 ± 0.20	1.216 ± 0.007	0.037 ± 0.000	6.854 ± 0.061	0.0313 ± 0.0002	17.57	1.45	70.90	0.09	150.9 ± 2.1
600	36.46 ± 0.20	1.445 ± 0.005	0.034 ± 0.000	6.503 ± 0.062	0.0342 ± 0.0003	18.65	1.72	73.70	0.11	159.8 ± 1.6
625	32.19 ± 0.09	1.289 ± 0.004	0.032 ± 0.001	6.127 ± 0.065	0.0321 ± 0.0003	18.04	1.53	72.00	0.11	154.8 ± 1.5
650	44.57 ± 0.14	1.641 ± 0.005	0.037 ± 0.002	6.507 ± 0.069	0.0496 ± 0.0003	18.59	1.95	68.30	0.13	159.3 ± 1.7
675	59.02 ± 0.19	2.147 ± 0.006	0.032 ± 0.000	5.303 ± 0.065	0.0552 ± 0.0003	20.11	2.55	73.00	0.21	171.7 ± 1.7
700	83.42 ± 0.26	3.274 ± 0.009	0.029 ± 0.000	4.946 ± 0.061	0.0425 ± 0.0003	21.78	3.89	85.40	0.34	185.2 ± 1.3
750	128.67 ± 0.55	4.776 ± 0.021	0.030 ± 0.004	4.214 ± 0.072	0.0457 ± 0.0003	24.19	5.68	89.80	0.58	204.7 ± 1.8
800	231.29 ± 1.46	7.316 ± 0.035	0.030 ± 0.001	4.329 ± 0.064	0.0545 ± 0.0003	29.47	8.70	93.20	0.86	246.3 ± 2.7
850	321.42 ± 0.65	8.529 ± 0.031	0.033 ± 0.001	3.937 ± 0.056	0.0461 ± 0.0002	36.13	10.14	95.90	1.11	297.6 ± 1.9
900	401.22 ± 0.83	9.967 ± 0.039	0.031 ± 0.001	3.623 ± 0.054	0.0325 ± 0.0002	39.32	11.85	97.70	1.40	321.8 ± 1.7
950	450.34 ± 1.89	10.891 ± 0.027	0.033 ± 0.001	3.326 ± 0.054	0.0190 ± 0.0002	40.86	12.95	98.80	1.67	333.2 ± 2.1
1000	346.40 ± 0.94	8.515 ± 0.021	0.026 ± 0.001	3.375 ± 0.053	0.0144 ± 0.0002	40.22	10.12	98.80	1.29	328.4 ± 1.9
1050	245.37 ± 1.35	6.417 ± 0.038	0.026 ± 0.000	2.851 ± 0.054	0.0125 ± 0.0002	37.70	7.63	98.60	1.15	309.5 ± 3.1
1100	158.62 ± 0.26	4.130 ± 0.012	0.022 ± 0.001	2.874 ± 0.055	0.0147 ± 0.0002	37.42	4.91	97.40	0.73	307.4 ± 1.6
1200	99.60 ± 0.17	3.524 ± 0.006	0.019 ± 0.000	2.492 ± 0.051	0.0187 ± 0.0002	26.76	4.19	94.70	0.72	225.1 ± 1.1
1350	5.74 ± 0.06	1.144 ± 0.002	0.015 ± 0.000	2.345 ± 0.051	0.0137 ± 0.0002	1.65	1.36	32.80	0.25	14.7 ± 0.5
1650	13.53 ± 0.07	0.890 ± 0.003	0.017 ± 0.000	2.456 ± 0.061	0.0297 ± 0.0003	5.57	1.06	36.60	0.18	49.2 ± 1.3
									Total fusion age = 253.6 Ma	
345 (2–6 μm) J = 0.00494 ± 0.5%; wt = 4.908 mg										
500	257.27 ± 6.40	5.292 ± 0.267	0.084 ± 0.005	9.029 ± 0.311	0.6646 ± 0.0037	11.64	5.88	23.90	0.30	100.9 ± 16.5
525	81.37 ± 1.15	1.751 ± 0.034	0.040 ± 0.001	7.321 ± 0.089	0.2244 ± 0.0009	8.94	1.95	19.20	0.12	78.0 ± 10.9
550	66.89 ± 0.74	1.611 ± 0.028	0.048 ± 0.001	8.979 ± 0.138	0.1733 ± 0.0007	10.20	1.79	24.50	0.09	88.7 ± 8.4
575	51.38 ± 0.45	1.765 ± 0.010	0.053 ± 0.001	10.396 ± 0.096	0.1141 ± 0.0004	10.51	1.96	36.00	0.09	91.3 ± 3.4
600	43.55 ± 0.23	1.841 ± 0.009	0.045 ± 0.001	8.787 ± 0.076	0.0828 ± 0.0004	10.76	2.05	45.40	0.11	93.5 ± 2.4
625	38.22 ± 0.14	1.865 ± 0.008	0.040 ± 0.000	7.481 ± 0.087	0.0677 ± 0.0004	10.10	2.07	49.20	0.13	87.9 ± 1.9
650	37.12 ± 0.13	1.768 ± 0.006	0.038 ± 0.000	6.868 ± 0.074	0.0659 ± 0.0003	10.31	1.97	49.00	0.13	89.6 ± 1.9
675	61.02 ± 0.27	2.988 ± 0.012	0.039 ± 0.000	7.204 ± 0.097	0.1011 ± 0.0004	10.62	3.32	51.90	0.21	92.2 ± 1.8
700	78.83 ± 0.34	4.527 ± 0.015	0.033 ± 0.001	6.091 ± 0.075	0.0751 ± 0.0003	12.62	5.03	72.40	0.38	109.1 ± 1.3
750	129.08 ± 0.48	7.305 ± 0.031	0.038 ± 0.001	5.798 ± 0.077	0.0727 ± 0.0005	14.79	8.12	83.70	0.64	127.2 ± 1.3
800	231.40 ± 1.59	10.589 ± 0.053	0.039 ± 0.001	5.678 ± 0.091	0.0788 ± 0.0005	19.70	11.77	90.10	0.95	167.5 ± 2.1
850	284.27 ± 1.34	10.653 ± 0.054	0.040 ± 0.001	4.659 ± 0.069	0.0479 ± 0.0003	25.39	11.84	95.10	1.17	213.2 ± 1.8
900	287.04 ± 1.48	10.709 ± 0.051	0.037 ± 0.001	4.570 ± 0.061	0.0278 ± 0.0002	26.07	11.90	97.30	1.20	218.5 ± 2.1
950	262.14 ± 1.55	9.482 ± 0.022	0.029 ± 0.001	4.401 ± 0.067	0.0160 ± 0.0002	27.18	10.54	98.30	1.10	227.3 ± 1.5
1000	182.00 ± 1.05	6.658 ± 0.037	0.028 ± 0.000	4.159 ± 0.060	0.0117 ± 0.0002	26.87	7.40	98.30	0.82	224.8 ± 2.1
1050	112.85 ± 0.40	4.074 ± 0.011	0.024 ± 0.001	3.870 ± 0.056	0.0098 ± 0.0002	27.07	4.53	97.70	0.54	226.5 ± 1.3
1100	88.36 ± 0.28	3.171 ± 0.008	0.021 ± 0.002	3.470 ± 0.057	0.0117 ± 0.0002	26.88	3.52	96.40	0.47	224.9 ± 1.4
1200	56.62 ± 0.15	2.795 ± 0.006	0.022 ± 0.000	3.271 ± 0.055	0.0179 ± 0.0002	18.46	3.11	91.10	0.44	157.4 ± 1.0
1350	3.42 ± 0.05	0.633 ± 0.002	0.016 ± 0.000	2.907 ± 0.052	0.0108 ± 0.0002	0.74	0.70	13.60	0.11	6.6 ± 0.7
1650	7.31 ± 0.07	0.513 ± 0.002	0.019 ± 0.000	3.447 ± 0.065	0.0208 ± 0.0002	2.77	0.57	19.40	0.08	24.5 ± 1.6
									Total fusion age = 169.2 Ma	

1345b (2–6 μm) J = 0.004943 ± 0.5%; wt = 3.812 mg

500	150.20 ± 5.19	5.511 ± 0.177	0.035 ± 0.001	1.754 ± 0.078	0.2369 ± 0.0014	14.57	7.43	53.50	1.60	125.5 ± 8.2
525	24.71 ± 0.59	1.291 ± 0.023	0.005 ± 0.001	0.107 ± 0.033	0.0386 ± 0.0007	10.31	1.74	53.90	6.16	89.7 ± 4.3
550	18.53 ± 0.40	1.001 ± 0.012	0.003 ± 0.001	0.146 ± 0.040	0.0306 ± 0.0008	9.49	1.35	51.30	3.50	82.7 ± 3.2
575	25.81 ± 0.45	1.458 ± 0.014	0.006 ± 0.001	0.473 ± 0.058	0.0401 ± 0.0011	9.60	1.97	54.20	1.57	83.7 ± 2.7
600	27.32 ± 0.33	1.502 ± 0.009	0.004 ± 0.001	0.621 ± 0.058	0.0384 ± 0.0010	10.66	2.03	58.60	1.23	92.7 ± 2.0
625	18.56 ± 0.24	1.005 ± 0.007	0.006 ± 0.001	0.717 ± 0.052	0.0278 ± 0.0008	10.34	1.36	56.00	0.72	89.9 ± 1.6
650	35.61 ± 0.29	1.885 ± 0.012	0.009 ± 0.001	1.085 ± 0.058	0.0584 ± 0.0009	9.77	2.54	51.70	0.89	85.1 ± 2.0
675	34.89 ± 0.29	1.561 ± 0.012	0.009 ± 0.001	1.067 ± 0.049	0.0580 ± 0.0008	11.43	2.10	51.10	0.75	99.1 ± 2.1
700	82.70 ± 0.69	3.852 ± 0.030	0.016 ± 0.001	1.199 ± 0.056	0.1137 ± 0.0010	12.77	5.19	59.50	1.64	110.4 ± 2.5
750	112.15 ± 0.69	5.836 ± 0.037	0.020 ± 0.001	1.156 ± 0.054	0.1034 ± 0.0010	13.99	7.87	72.80	2.58	120.6 ± 1.7
800	186.03 ± 1.24	8.297 ± 0.040	0.018 ± 0.001	1.185 ± 0.051	0.0998 ± 0.0009	18.87	11.19	84.20	3.57	160.9 ± 2.0
850	242.74 ± 1.36	9.454 ± 0.051	0.027 ± 0.001	0.902 ± 0.052	0.0630 ± 0.0009	23.71	12.75	92.40	5.35	199.9 ± 2.3
900	229.34 ± 1.29	8.254 ± 0.036	0.017 ± 0.001	0.915 ± 0.047	0.0304 ± 0.0008	26.70	11.13	96.10	4.60	223.7 ± 1.8
950	230.59 ± 1.37	8.337 ± 0.034	0.019 ± 0.001	0.991 ± 0.048	0.0162 ± 0.0008	27.09	11.24	98.00	4.29	226.7 ± 2.0
1000	171.29 ± 1.02	6.432 ± 0.023	0.011 ± 0.001	0.973 ± 0.046	0.0113 ± 0.0007	26.12	8.67	98.10	3.37	219.1 ± 1.9
1050	106.14 ± 0.30	3.743 ± 0.010	0.010 ± 0.001	0.872 ± 0.047	0.0095 ± 0.0008	27.62	5.05	97.40	2.19	230.9 ± 1.3
1100	69.64 ± 0.31	2.528 ± 0.013	0.010 ± 0.001	0.831 ± 0.047	0.0094 ± 0.0008	26.47	3.41	96.10	1.55	221.8 ± 1.7
1200	32.33 ± 0.27	1.801 ± 0.005	0.008 ± 0.001	0.800 ± 0.044	0.0122 ± 0.0007	15.98	2.43	89.00	1.15	137.2 ± 1.2
1350	0.57 ± 0.04	0.121 ± 0.001	0.001 ± 0.000	0.155 ± 0.010	0.0015 ± 0.0002	1.08	0.16	23.10	0.40	9.6 ± 0.7
1650	3.68 ± 0.17	0.299 ± 0.004	0.005 ± 0.000	0.577 ± 0.038	0.0093 ± 0.0006	3.23	0.40	26.20	0.26	28.6 ± 1.5
									Total fusion age = 167.2 Ma	

367 (2–6 μm) J = 0.004965 ± 0.5%; wt = 3.171 mg

500	92.14 ± 0.89	3.600 ± 0.031	0.017 ± 0.001	0.770 ± 0.049	0.2409 ± 0.0010	5.83	3.73	22.80	2.39	51.5 ± 3.7
525	13.79 ± 0.13	0.545 ± 0.006	0.002 ± 0.000	0.178 ± 0.031	0.0305 ± 0.0005	8.79	0.57	34.80	1.56	77.1 ± 3.4
550	13.96 ± 0.20	0.612 ± 0.009	0.002 ± 0.000	0.177 ± 0.028	0.0265 ± 0.0005	10.06	0.63	44.10	1.76	87.9 ± 3.8
575	18.97 ± 0.21	1.107 ± 0.008	0.004 ± 0.000	0.153 ± 0.036	0.0327 ± 0.0005	8.43	1.15	49.20	3.69	73.9 ± 2.1
600	23.85 ± 0.17	1.580 ± 0.008	0.005 ± 0.000	0.222 ± 0.036	0.0333 ± 0.0005	8.87	1.64	58.80	3.63	77.7 ± 1.4
625	29.86 ± 0.15	2.113 ± 0.008	0.006 ± 0.000	0.313 ± 0.037	0.0369 ± 0.0005	8.98	2.19	63.60	3.45	78.7 ± 1.1
650	36.66 ± 0.16	2.658 ± 0.012	0.008 ± 0.001	0.242 ± 0.039	0.0439 ± 0.0005	8.90	2.75	64.60	5.61	78.0 ± 1.1
675	33.50 ± 0.13	2.260 ± 0.006	0.005 ± 0.000	0.231 ± 0.034	0.0428 ± 0.0005	9.22	2.34	62.20	4.99	80.8 ± 1.0
700	56.77 ± 0.27	4.222 ± 0.011	0.007 ± 0.002	0.332 ± 0.038	0.0507 ± 0.0005	9.90	4.38	73.60	6.48	86.6 ± 0.9
750	110.79 ± 0.56	8.255 ± 0.038	0.008 ± 0.001	0.388 ± 0.041	0.0911 ± 0.0005	10.16	8.55	75.70	10.85	88.8 ± 1.1
800	213.58 ± 1.12	15.111 ± 0.049	0.026 ± 0.001	0.468 ± 0.042	0.1494 ± 0.0006	11.21	15.66	79.30	16.47	97.7 ± 0.9
850	247.85 ± 0.75	17.342 ± 0.065	0.017 ± 0.001	0.298 ± 0.037	0.0838 ± 0.0005	12.86	17.97	90.00	29.71	111.6 ± 1.0
900	263.11 ± 1.10	14.800 ± 0.033	0.022 ± 0.001	0.219 ± 0.032	0.0437 ± 0.0005	16.90	15.34	95.10	34.54	145.4 ± 0.8
1000	378.89 ± 0.70	14.882 ± 0.039	0.017 ± 0.002	0.119 ± 0.030	0.0274 ± 0.0004	24.91	15.42	97.90	63.54	210.4 ± 1.2
1100	142.32 ± 0.73	4.307 ± 0.012	0.005 ± 0.001	0.069 ± 0.030	0.0096 ± 0.0004	32.38	4.46	98.00	32.02	269.0 ± 1.9
1200	56.47 ± 0.26	2.141 ± 0.007	0.002 ± 0.000	0.021 ± 0.041	0.0065 ± 0.0004	25.47	2.22	96.60	51.97	214.9 ± 1.5
1350	1.75 ± 0.06	0.447 ± 0.002	0.001 ± 0.000	0.002 ± 0.028	0.0020 ± 0.0003	2.60	0.46	66.30	144.81	23.1 ± 0.4
1650	5.77 ± 0.10	0.518 ± 0.003	0.004 ± 0.001	0.015 ± 0.033	0.0113 ± 0.0004	4.69	0.54	42.20	17.59	41.6 ± 1.0
									Total fusion age = 128.2 Ma	

Table 1 (contd.)

T (°C)	^{40}Ar $\times 10^{-14}$moles	^{39}Ar $\times 10^{-14}$ moles	^{38}Ar $\times 10^{-14}$ moles	^{37}Ar $\times 10^{-14}$ moles	^{36}Ar $\times 10^{-14}$ moles	$^{40}Ar^{a}/^{39}Ar$	$\%^{39}Ar_{K}$	$\%^{40}Ar^{a}$	K/Ca	Age $\pm 2\sigma$
253 (2–6 μm) J = 0.004945 ± 0.5%; wt = 3.675 mg										
500	33.55 ± 0.25	1.256 ± 0.013	0.006 ± 0.000	0.461 ± 0.055	0.0847 ± 0.0003	6.81	1.48	25.50	1.39	59.8 ± 4.0
525	3.15 ± 0.04	0.076 ± 0.001	0.001 ± 0.000	0.121 ± 0.025	0.0081 ± 0.0001	10.04	0.09	24.00	0.32	87.4 ± 7.1
550	3.23 ± 0.04	0.097 ± 0.001	0.001 ± 0.000	0.022 ± 0.033	0.0077 ± 0.0001	9.92	0.11	29.60	2.21	86.4 ± 4.1
575	5.59 ± 0.06	0.204 ± 0.002	0.001 ± 0.000	0.090 ± 0.037	0.0133 ± 0.0002	8.20	0.24	30.00	1.15	71.7 ± 3.5
600	10.15 ± 0.08	0.458 ± 0.002	0.002 ± 0.000	0.214 ± 0.045	0.0234 ± 0.0002	7.11	0.54	32.10	1.09	62.3 ± 2.4
625	14.59 ± 0.08	0.586 ± 0.004	0.003 ± 0.000	0.330 ± 0.049	0.0356 ± 0.0002	6.97	0.69	28.00	0.91	61.1 ± 2.9
650	26.14 ± 0.18	0.941 ± 0.003	0.004 ± 0.000	0.249 ± 0.054	0.0628 ± 0.0003	8.07	1.11	29.10	1.93	70.6 ± 3.0
675	14.27 ± 0.11	0.698 ± 0.005	0.002 ± 0.000	0.130 ± 0.047	0.0286 ± 0.0002	8.34	0.82	40.80	2.75	72.9 ± 2.5
700	20.28 ± 0.13	1.559 ± 0.006	0.002 ± 0.000	0.199 ± 0.052	0.0243 ± 0.0002	8.41	1.83	64.70	3.99	73.5 ± 1.2
750	30.67 ± 0.13	2.695 ± 0.015	0.005 ± 0.000	0.241 ± 0.052	0.0155 ± 0.0002	9.69	3.17	85.20	5.70	84.4 ± 0.9
800	105.37 ± 0.55	9.635 ± 0.027	0.015 ± 0.001	0.178 ± 0.052	0.0264 ± 0.0002	10.12	11.32	92.60	27.59	88.1 ± 0.8
850	176.61 ± 0.53	15.145 ± 0.039	0.017 ± 0.001	0.131 ± 0.066	0.0218 ± 0.0002	11.23	17.80	96.30	59.11	97.5 ± 0.6
900	250.32 ± 0.89	17.404 ± 0.038	0.026 ± 0.002	0.025 ± 0.072	0.0174 ± 0.0002	14.08	20.45	97.90	360.05	121.4 ± 0.7
950	228.11 ± 0.83	14.986 ± 0.057	0.030 ± 0.002	0.000 ± 0.000	0.0114 ± 0.0002	14.99	17.61	98.50	0.00	129.0 ± 1.0
1000	169.30 ± 0.58	9.459 ± 0.028	0.017 ± 0.001	0.000 ± 0.000	0.0077 ± 0.0002	17.65	11.12	98.60	0.00	150.9 ± 1.0
1050	101.82 ± 0.22	4.843 ± 0.016	0.007 ± 0.001	0.000 ± 0.000	0.0047 ± 0.0002	20.73	5.69	98.60	0.00	176.1 ± 1.2
1100	63.86 ± 0.21	3.072 ± 0.008	0.003 ± 0.001	0.000 ± 0.000	0.0046 ± 0.0002	20.34	3.61	97.90	0.00	172.9 ± 1.1
1200	29.54 ± 0.11	1.471 ± 0.003	0.002 ± 0.000	0.000 ± 0.000	0.0048 ± 0.0002	19.10	1.73	95.20	0.00	162.8 ± 0.9
1350	1.57 ± 0.05	0.259 ± 0.001	0.001 ± 0.000	0.000 ± 0.000	0.0027 ± 0.0002	3.02	0.30	49.70	0.00	26.7 ± 0.8
1650	4.43 ± 0.07	0.255 ± 0.002	0.002 ± 0.000	0.000 ± 0.000	0.0106 ± 0.0002	5.13	0.30	29.50	0.00	45.2 ± 1.8
									Total fusion age = 117.7 Ma	
26 (2–6 μm) J = 0.00495 ± 0.5%; wt = 3.029 mg										
500	220.62 ± 0.87	1.122 ± 0.019	0.020 ± 0.001	1.200 ± 0.081	0.6847 ± 0.0019	16.36	0.65	8.30	0.48	140.5 ± 33.7
525	43.56 ± 0.28	0.637 ± 0.006	0.008 ± 0.001	0.827 ± 0.070	0.1345 ± 0.0005	6.10	0.37	8.90	0.39	53.6 ± 10.6
550	29.07 ± 0.17	0.737 ± 0.007	0.008 ± 0.000	0.873 ± 0.067	0.0864 ± 0.0004	4.88	0.43	12.40	0.43	43.1 ± 5.9
575	15.89 ± 0.11	0.688 ± 0.004	0.005 ± 0.000	0.565 ± 0.057	0.0417 ± 0.0003	5.24	0.40	22.70	0.62	46.2 ± 3.1
600	14.07 ± 0.10	0.793 ± 0.004	0.004 ± 0.000	0.593 ± 0.063	0.0310 ± 0.0003	6.27	0.46	35.30	0.68	55.1 ± 2.0
625	13.86 ± 0.08	0.825 ± 0.003	0.005 ± 0.000	0.667 ± 0.061	0.0309 ± 0.0002	5.77	0.48	34.40	0.63	50.8 ± 1.6
650	13.50 ± 0.09	0.676 ± 0.004	0.005 ± 0.000	0.775 ± 0.062	0.0325 ± 0.0002	5.84	0.39	29.20	0.45	51.4 ± 2.3
675	16.13 ± 0.10	0.986 ± 0.005	0.005 ± 0.000	0.713 ± 0.061	0.0362 ± 0.0002	5.56	0.57	34.00	0.71	49.0 ± 1.8
700	13.88 ± 0.08	1.831 ± 0.007	0.006 ± 0.000	0.622 ± 0.061	0.0137 ± 0.0002	5.39	1.07	71.10	1.50	47.5 ± 0.6
750	27.66 ± 0.19	4.367 ± 0.022	0.011 ± 0.001	0.935 ± 0.068	0.0069 ± 0.0002	5.88	2.54	92.90	2.38	51.7 ± 0.6
800	65.62 ± 0.25	10.099 ± 0.021	0.012 ± 0.001	0.702 ± 0.065	0.0079 ± 0.0002	6.26	5.88	96.50	7.34	55.1 ± 0.4
850	142.66 ± 0.60	20.546 ± 0.096	0.025 ± 0.002	0.413 ± 0.058	0.0113 ± 0.0002	6.78	11.97	97.70	25.40	59.5 ± 0.5
900	235.17 ± 0.59	32.091 ± 0.070	0.043 ± 0.002	0.205 ± 0.050	0.0142 ± 0.0002	7.19	18.70	98.20	79.82	63.1 ± 0.4
950	337.34 ± 1.42	41.327 ± 0.100	0.046 ± 0.003	0.288 ± 0.052	0.0177 ± 0.0002	8.03	24.08	98.40	73.20	70.3 ± 0.5
1000	305.00 ± 0.77	32.372 ± 0.105	0.033 ± 0.002	0.196 ± 0.054	0.0131 ± 0.0002	9.30	18.86	98.70	84.12	81.2 ± 0.6
1050	164.05 ± 0.43	14.032 ± 0.037	0.016 ± 0.001	0.075 ± 0.045	0.0062 ± 0.0002	11.55	8.18	98.90	95.86	100.3 ± 0.6
1100	85.33 ± 0.26	5.532 ± 0.015	0.007 ± 0.000	0.083 ± 0.046	0.0035 ± 0.0002	15.23	3.22	98.80	34.14	131.1 ± 0.8
1200	51.29 ± 0.19	2.682 ± 0.010	0.004 ± 0.000	0.097 ± 0.047	0.0024 ± 0.0002	18.85	1.56	98.60	14.14	161.0 ± 1.2
1350	3.45 ± 0.05	0.169 ± 0.002	0.001 ± 0.000	0.061 ± 0.073	0.0009 ± 0.0002	18.85	0.10	92.50	1.40	160.9 ± 1.2
1650	2.45 ± 0.07	0.110 ± 0.002	0.002 ± 0.000	0.305 ± 0.051	0.0056 ± 0.0002	7.38	0.06	33.30	0.18	64.8 ± 2.5
									Total fusion age = 73.8 Ma	

33 (2–6 μm) J = 0.00494 ± 0.5%; wt = 4.041 mg

500	226.03 ± 2.58	1.490 ± 0.035	0.020 ± 0.001	0.650 ± 0.020	0.6630 ± 0.0039	20.24	0.78	13.30	1.17	171.9 ± 34.0
525	45.68 ± 0.19	0.673 ± 0.011	0.008 ± 0.000	0.420 ± 0.026	0.1336 ± 0.0007	9.25	0.35	13.60	0.82	80.6 ± 11.7
550	31.18 ± 0.29	0.585 ± 0.008	0.005 ± 0.000	0.374 ± 0.011	0.0903 ± 0.0004	7.73	0.31	14.50	0.80	67.6 ± 10.0
575	23.41 ± 0.21	0.725 ± 0.007	0.005 ± 0.000	0.390 ± 0.011	0.0649 ± 0.0003	5.88	0.38	18.20	0.95	51.7 ± 5.0
600	15.72 ± 0.16	0.783 ± 0.007	0.004 ± 0.000	0.427 ± 0.014	0.0370 ± 0.0003	6.15	0.41	30.60	0.94	54.0 ± 3.3
625	14.04 ± 0.11	0.808 ± 0.005	0.004 ± 0.000	0.378 ± 0.011	0.0303 ± 0.0002	6.31	0.42	36.30	1.09	55.4 ± 2.2
650	15.14 ± 0.08	0.815 ± 0.003	0.005 ± 0.000	0.409 ± 0.015	0.0334 ± 0.0002	6.51	0.43	35.00	1.02	57.1 ± 2.0
675	12.38 ± 0.14	0.564 ± 0.005	0.000 ± 0.004	0.281 ± 0.009	0.0280 ± 0.0002	7.31	0.29	33.30	1.02	64.0 ± 3.8
700	21.56 ± 0.06	1.215 ± 0.003	0.004 ± 0.000	0.364 ± 0.009	0.0469 ± 0.0003	6.34	0.64	35.80	1.70	55.7 ± 1.7
750	28.76 ± 0.12	3.444 ± 0.011	0.011 ± 0.000	0.487 ± 0.010	0.0160 ± 0.0002	6.98	1.80	83.70	3.61	61.2 ± 0.6
800	66.20 ± 0.36	10.326 ± 0.036	0.011 ± 0.001	0.532 ± 0.017	0.0130 ± 0.0002	6.04	5.40	94.20	9.89	53.0 ± 0.5
850	166.31 ± 1.38	25.318 ± 0.217	0.045 ± 0.002	0.580 ± 0.022	0.0312 ± 0.0003	6.20	13.23	94.50	22.29	54.4 ± 0.8
900	308.83 ± 1.68	35.338 ± 0.072	0.035 ± 0.001	0.492 ± 0.015	0.0338 ± 0.0002	8.45	18.47	96.80	36.68	73.8 ± 0.4
950	435.10 ± 0.96	46.207 ± 0.136	0.045 ± 0.003	0.500 ± 0.012	0.0345 ± 0.0002	9.19	24.15	97.60	47.11	80.1 ± 0.4
1000	414.13 ± 1.19	39.022 ± 0.140	0.043 ± 0.003	0.415 ± 0.011	0.0221 ± 0.0002	10.44	20.39	98.40	48.03	90.7 ± 0.7
1050	217.44 ± 0.84	16.139 ± 0.053	0.014 ± 0.000	0.412 ± 0.011	0.0128 ± 0.0002	13.23	8.43	98.30	19.99	114.2 ± 0.8
1100	95.47 ± 0.33	5.311 ± 0.021	0.007 ± 0.000	0.360 ± 0.011	0.0071 ± 0.0002	17.58	2.78	97.80	7.52	150.2 ± 1.2
1200	56.94 ± 0.16	2.312 ± 0.004	0.006 ± 0.002	0.414 ± 0.011	0.0054 ± 0.0002	23.95	1.21	97.30	2.85	201.7 ± 1.0
1350	1.18 ± 0.02	0.122 ± 0.001	0.002 ± 0.000	0.331 ± 0.008	0.0003 ± 0.0001	9.11	0.06	93.70	0.19	79.4 ± 1.3
1650	2.38 ± 0.03	0.156 ± 0.001	0.003 ± 0.000	0.362 ± 0.010	0.0048 ± 0.0001	6.30	0.08	41.20	0.22	55.3 ± 2.0
									Total fusion age = 82.5 Ma	

33 (6–20 μm) J = 0.00495 ± 0.5%; wt = 4.889 mg

500	154.40 ± 1.41	1.436 ± 0.044	0.017 ± 0.002	1.209 ± 0.068	0.4815 ± 0.0011	8.49	2.68	7.90	0.61	74.3 ± 24.2
525	28.15 ± 0.49	0.718 ± 0.016	0.007 ± 0.000	0.890 ± 0.064	0.0689 ± 0.0003	10.94	1.34	27.90	0.41	95.1 ± 7.6
550	25.33 ± 0.20	0.682 ± 0.009	0.005 ± 0.000	0.452 ± 0.057	0.0468 ± 0.0003	16.89	1.28	45.50	0.77	144.9 ± 4.2
575	21.87 ± 0.13	0.654 ± 0.004	0.004 ± 0.000	0.326 ± 0.059	0.0336 ± 0.0002	18.32	1.22	54.70	1.02	156.6 ± 2.7
600	25.15 ± 0.11	0.765 ± 0.003	0.004 ± 0.000	0.275 ± 0.059	0.0342 ± 0.0003	19.68	1.43	59.90	1.42	167.7 ± 2.2
625	26.09 ± 0.18	0.765 ± 0.005	0.005 ± 0.000	0.361 ± 0.064	0.0348 ± 0.0002	20.67	1.43	60.60	1.08	175.8 ± 3.5
650	24.30 ± 0.12	0.633 ± 0.003	0.004 ± 0.000	0.234 ± 0.060	0.0363 ± 0.0002	21.48	1.18	55.90	1.38	182.3 ± 3.0
675	33.38 ± 0.12	0.883 ± 0.003	0.004 ± 0.000	0.285 ± 0.059	0.0490 ± 0.0002	21.44	1.65	56.70	1.58	182.0 ± 2.5
700	56.42 ± 0.27	1.799 ± 0.007	0.006 ± 0.001	0.404 ± 0.063	0.0510 ± 0.0002	23.00	3.36	73.30	2.27	194.5 ± 2.2
750	73.11 ± 0.27	2.600 ± 0.010	0.008 ± 0.000	0.481 ± 0.064	0.0393 ± 0.0002	23.66	4.86	84.20	2.76	199.8 ± 1.7
800	123.14 ± 0.57	4.041 ± 0.018	0.009 ± 0.001	0.465 ± 0.064	0.0449 ± 0.0002	27.20	7.55	89.30	4.43	227.9 ± 2.0
850	155.67 ± 0.69	4.622 ± 0.018	0.011 ± 0.001	0.394 ± 0.061	0.0346 ± 0.0002	31.47	8.64	93.50	5.98	261.2 ± 2.2
900	698.14 ± 2.62	18.814 ± 0.059	0.021 ± 0.002	0.307 ± 0.053	0.0509 ± 0.0003	36.30	35.17	97.80	31.27	298.1 ± 1.9
950	3.57 ± 0.05	0.103 ± 0.002	0.001 ± 0.000	0.077 ± 0.050	0.0007 ± 0.0002	32.60	0.19	94.10	0.68	269.9 ± 2.8
1000	15.14 ± 0.06	0.402 ± 0.002	0.001 ± 0.000	0.051 ± 0.052	0.0008 ± 0.0002	37.11	0.75	98.50	3.98	304.3 ± 1.4
1050	66.12 ± 0.12	1.720 ± 0.003	0.004 ± 0.000	0.000 ± 0.000	0.0035 ± 0.0002	37.84	3.21	98.40	0.00	309.7 ± 1.4
1100	142.86 ± 0.34	3.695 ± 0.009	0.007 ± 0.003	0.000 ± 0.000	0.0091 ± 0.0002	37.93	6.91	98.10	0.00	310.4 ± 1.7
1200	249.45 ± 1.09	6.919 ± 0.024	0.007 ± 0.001	0.000 ± 0.000	0.0263 ± 0.0002	34.92	12.93	96.90	0.00	287.7 ± 2.0
1350	29.56 ± 0.10	1.316 ± 0.003	0.003 ± 0.001	0.024 ± 0.067	0.0150 ± 0.0002	19.09	2.46	85.00	28.23	162.9 ± 1.1
1650	29.29 ± 0.08	0.930 ± 0.003	0.006 ± 0.001	0.000 ± 0.000	0.0476 ± 0.0003	16.38	1.74	52.00	0.00	140.6 ± 2.1
									Total fusion age = 255.2 Ma	

Table 1 (Contd.)

T (°C)	^{40}Ar $\times 10^{-14}$moles	^{39}Ar $\times 10^{-14}$ moles	^{38}Ar $\times 10^{-14}$ moles	^{37}Ar $\times 10^{-14}$ moles	^{36}Ar $\times 10^{-14}$ moles	$^{40}Ar^a/^{39}Ar$	$\%^{39}Ar_K$	$\%^{40}Ar^a$	K/Ca	Age $\pm 2\sigma$
345 (6–20 μm) J = 0.004935 ± 0.5%; wt = 5.218 mg										
500	161.40 ± 4.75	4.996 ± 0.177	0.045 ± 0.001	6.011 ± 0.264	0.3037 ± 0.0012	14.44	6.05	44.70	0.42	124.2 ± 8.7
525	24.52 ± 0.73	1.236 ± 0.024	0.019 ± 0.001	2.857 ± 0.112	0.0445 ± 0.0003	9.39	1.50	47.20	0.22	81.7 ± 5.0
550	27.13 ± 0.25	1.527 ± 0.008	0.026 ± 0.000	4.863 ± 0.099	0.0455 ± 0.0003	9.23	1.85	51.80	0.16	80.4 ± 2.0
575	26.53 ± 0.20	1.386 ± 0.009	0.028 ± 0.000	5.442 ± 0.086	0.0412 ± 0.0003	10.69	1.68	55.70	0.13	92.7 ± 2.3
600	28.43 ± 0.20	1.567 ± 0.012	0.026 ± 0.000	4.740 ± 0.079	0.0398 ± 0.0003	10.90	1.90	60.00	0.17	94.5 ± 2.1
625	31.93 ± 0.28	1.804 ± 0.010	0.029 ± 0.000	5.164 ± 0.075	0.0478 ± 0.0003	10.10	2.19	57.00	0.18	87.8 ± 2.0
650	36.53 ± 0.18	2.094 ± 0.011	0.027 ± 0.000	5.070 ± 0.073	0.0494 ± 0.0003	10.68	2.54	61.10	0.21	92.6 ± 1.6
675	34.23 ± 0.23	2.135 ± 0.011	0.026 ± 0.001	4.854 ± 0.081	0.0354 ± 0.0003	11.32	2.59	70.50	0.22	98.0 ± 1.5
700	69.10 ± 0.31	4.293 ± 0.019	0.030 ± 0.001	4.406 ± 0.057	0.0481 ± 0.0003	12.87	5.20	79.90	0.50	111.1 ± 1.3
750	102.49 ± 0.60	6.025 ± 0.037	0.026 ± 0.001	4.114 ± 0.069	0.0539 ± 0.0003	14.42	7.30	84.80	0.75	124.0 ± 1.8
800	180.98 ± 1.04	8.705 ± 0.046	0.030 ± 0.002	3.573 ± 0.057	0.0611 ± 0.0004	18.75	10.54	90.20	1.24	159.6 ± 1.8
850	229.87 ± 1.95	9.478 ± 0.048	0.036 ± 0.002	3.495 ± 0.068	0.0412 ± 0.0003	23.00	11.48	94.80	1.38	193.9 ± 2.2
900	212.80 ± 1.12	8.228 ± 0.040	0.028 ± 0.001	3.127 ± 0.061	0.0226 ± 0.0002	25.08	9.97	97.00	1.34	210.5 ± 1.9
950	169.48 ± 0.71	6.822 ± 0.028	0.019 ± 0.001	2.883 ± 0.055	0.0118 ± 0.0002	24.36	8.26	98.10	1.21	204.8 ± 1.6
1000	116.96 ± 0.74	4.832 ± 0.020	0.019 ± 0.001	2.568 ± 0.058	0.0083 ± 0.0002	23.74	5.85	98.10	0.96	199.9 ± 1.7
1050	114.33 ± 0.56	4.460 ± 0.015	0.020 ± 0.004	2.488 ± 0.055	0.0078 ± 0.0002	25.16	5.40	98.20	0.91	211.2 ± 1.4
1100	140.37 ± 0.40	5.460 ± 0.020	0.021 ± 0.001	2.240 ± 0.052	0.0113 ± 0.0002	25.13	6.61	97.70	1.24	210.9 ± 1.4
1200	146.35 ± 0.61	6.144 ± 0.025	0.019 ± 0.001	2.438 ± 0.057	0.0271 ± 0.0002	22.55	7.44	94.70	1.29	190.3 ± 1.3
1350	11.52 ± 0.06	0.861 ± 0.002	0.014 ± 0.001	2.127 ± 0.050	0.0149 ± 0.0002	8.48	1.04	63.30	0.21	73.9 ± 0.9
1650	15.04 ± 0.07	0.508 ± 0.002	0.015 ± 0.001	2.467 ± 0.064	0.0314 ± 0.0003	11.76	0.61	39.60	0.11	101.8 ± 2.4
									Total fusion age = 162.5 Ma	
367 (6–20 μm) J = 0.00495 ± 0.5%; wt = 4.517 mg										
500	227.52 ± 7.52	8.882 ± 0.320	0.066 ± 0.003	4.560 ± 0.176	0.5141 ± 0.0022	14.18	5.63	45.40	0.99	122.4 ± 10.0
525	41.90 ± 0.92	2.560 ± 0.035	0.028 ± 0.001	4.535 ± 0.091	0.0865 ± 0.0005	6.52	1.62	39.80	0.29	57.3 ± 3.4
550	43.53 ± 0.69	2.707 ± 0.035	0.043 ± 0.001	7.571 ± 0.101	0.0978 ± 0.0005	5.62	1.72	34.90	0.18	49.5 ± 3.1
575	50.95 ± 0.58	3.570 ± 0.035	0.047 ± 0.001	8.117 ± 0.158	0.0902 ± 0.0005	6.99	2.26	48.90	0.22	61.4 ± 2.4
600	54.82 ± 0.39	4.213 ± 0.038	0.052 ± 0.001	8.742 ± 0.113	0.0748 ± 0.0005	7.93	2.67	60.90	0.25	69.5 ± 1.9
625	56.47 ± 0.48	4.830 ± 0.023	0.053 ± 0.004	7.898 ± 0.124	0.0624 ± 0.0004	8.00	3.06	68.40	0.31	70.1 ± 1.2
650	32.15 ± 0.24	3.008 ± 0.015	0.038 ± 0.002	6.207 ± 0.084	0.0295 ± 0.0003	7.96	1.91	74.40	0.25	69.7 ± 1.1
675	43.59 ± 0.23	4.295 ± 0.019	0.038 ± 0.001	5.237 ± 0.073	0.0312 ± 0.0003	8.10	2.72	79.80	0.42	70.9 ± 0.8
700	100.70 ± 0.67	9.869 ± 0.053	0.041 ± 0.001	5.921 ± 0.089	0.0611 ± 0.0004	8.42	6.26	82.50	0.85	73.6 ± 1.1
750	174.18 ± 0.55	15.915 ± 0.055	0.038 ± 0.001	4.939 ± 0.076	0.0907 ± 0.0004	9.28	10.09	84.80	1.64	81.0 ± 0.7
800	278.04 ± 1.59	24.538 ± 0.148	0.050 ± 0.002	4.548 ± 0.082	0.1111 ± 0.0005	10.00	15.56	88.30	2.75	87.2 ± 1.1
850	361.06 ± 2.24	29.467 ± 0.142	0.064 ± 0.003	4.228 ± 0.080	0.0985 ± 0.0004	11.27	18.69	92.00	3.56	97.9 ± 1.0
900	312.87 ± 1.04	19.642 ± 0.062	0.051 ± 0.002	3.864 ± 0.070	0.0475 ± 0.0003	15.22	12.46	95.60	2.59	131.1 ± 0.8
950	215.88 ± 0.77	9.659 ± 0.038	0.032 ± 0.001	3.281 ± 0.074	0.0195 ± 0.0002	21.78	6.13	97.40	1.50	184.7 ± 1.4
1000	137.11 ± 0.64	4.808 ± 0.020	0.026 ± 0.001	3.602 ± 0.076	0.0108 ± 0.0002	27.92	3.05	97.90	0.68	233.6 ± 1.8
1050	89.31 ± 0.63	2.760 ± 0.015	0.025 ± 0.001	3.419 ± 0.088	0.0081 ± 0.0002	31.61	1.75	97.60	0.41	262.2 ± 2.4
1100	75.39 ± 0.33	2.182 ± 0.006	0.020 ± 0.001	2.928 ± 0.076	0.0007 ± 0.0002	33.63	1.38	97.30	0.38	277.8 ± 1.8
1200	104.77 ± 0.18	3.546 ± 0.007	0.021 ± 0.001	2.576 ± 0.078	0.0105 ± 0.0002	28.74	2.25	97.20	0.70	239.9 ± 1.1
1350	7.70 ± 0.03	0.768 ± 0.002	0.011 ± 0.001	1.808 ± 0.059	0.0071 ± 0.0002	7.50	0.49	74.60	0.22	65.7 ± 0.6
1650	12.69 ± 0.05	0.448 ± 0.003	0.015 ± 0.001	2.163 ± 0.075	0.0253 ± 0.0002	12.09	0.28	42.50	0.11	104.9 ± 2.5
									Total fusion age = 110.3 Ma	

253 (6–20 μm) J = 0.004945 ± 0.5%; wt = 4.008 mg

500	144.19 ± 1.34	1.118 ± 0.045	0.020 ± 0.001	2.053 ± 0.091	0.4616 ± 0.0011	7.11	1.53	5.50	0.28	62.4 ± 34.8
525	12.33 ± 0.23	0.414 ± 0.008	0.007 ± 0.001	1.022 ± 0.056	0.0312 ± 0.0002	7.73	0.57	25.90	0.21	67.7 ± 6.3
550	8.69 ± 0.13	0.366 ± 0.004	0.005 ± 0.000	0.872 ± 0.047	0.0200 ± 0.0002	7.79	0.50	32.70	0.21	68.2 ± 4.1
575	7.15 ± 0.07	0.351 ± 0.003	0.004 ± 0.000	0.698 ± 0.046	0.0158 ± 0.0002	7.25	0.48	35.60	0.26	63.6 ± 2.5
600	6.05 ± 0.04	0.353 ± 0.002	0.003 ± 0.001	0.407 ± 0.047	0.0120 ± 0.0002	7.20	0.48	41.90	0.44	63.2 ± 2.0
625	8.01 ± 0.07	0.386 ± 0.002	0.003 ± 0.001	0.547 ± 0.049	0.0174 ± 0.0002	7.55	0.53	36.30	0.36	66.2 ± 2.4
650	9.18 ± 0.05	0.340 ± 0.002	0.003 ± 0.001	0.356 ± 0.052	0.0222 ± 0.0002	7.77	0.47	28.80	0.49	68.1 ± 2.8
675	14.95 ± 0.05	0.608 ± 0.002	0.004 ± 0.001	0.424 ± 0.059	0.0352 ± 0.0002	7.55	0.83	30.70	0.73	66.2 ± 2.2
700	17.82 ± 0.07	1.268 ± 0.004	0.004 ± 0.001	0.396 ± 0.063	0.0260 ± 0.0002	8.02	1.74	57.10	1.63	70.2 ± 1.1
750	28.32 ± 0.10	3.016 ± 0.011	0.008 ± 0.001	0.551 ± 0.068	0.0103 ± 0.0002	8.39	4.14	89.40	2.79	73.4 ± 0.6
800	75.30 ± 0.09	8.018 ± 0.024	0.009 ± 0.001	0.489 ± 0.071	0.0131 ± 0.0002	8.91	11.00	94.90	8.37	77.8 ± 0.4
850	148.62 ± 0.72	13.639 ± 0.067	0.020 ± 0.001	0.602 ± 0.073	0.0131 ± 0.0002	10.61	18.71	97.40	11.55	92.3 ± 0.6
900	178.28 ± 0.59	13.532 ± 0.034	0.021 ± 0.001	0.531 ± 0.071	0.0103 ± 0.0002	12.94	18.56	98.30	13.01	112.0 ± 0.7
950	149.71 ± 0.33	9.949 ± 0.043	0.014 ± 0.001	0.489 ± 0.070	0.0061 ± 0.0002	14.86	13.64	98.80	10.37	128.1 ± 1.1
1000	108.35 ± 0.39	6.184 ± 0.024	0.009 ± 0.001	0.460 ± 0.071	0.0040 ± 0.0002	17.33	8.48	98.90	6.85	148.5 ± 1.2
1050	101.35 ± 0.22	4.549 ± 0.015	0.009 ± 0.001	0.448 ± 0.074	0.0030 ± 0.0002	22.08	6.24	99.10	5.19	187.2 ± 1.2
1100	112.04 ± 0.26	4.445 ± 0.009	0.010 ± 0.001	0.416 ± 0.072	0.0038 ± 0.0002	24.95	6.10	99.00	5.45	210.1 ± 1.0
1200	115.41 ± 0.60	3.911 ± 0.014	0.006 ± 0.001	0.449 ± 0.074	0.0057 ± 0.0002	29.08	5.36	98.60	4.45	242.6 ± 2.1
1350	5.70 ± 0.03	0.272 ± 0.001	0.002 ± 0.001	0.305 ± 0.052	0.0020 ± 0.0001	18.85	0.37	89.80	0.46	160.9 ± 1.2
1650	4.60 ± 0.03	0.196 ± 0.001	0.003 ± 0.001	0.354 ± 0.055	0.0077 ± 0.0002	12.07	0.27	51.40	0.28	104.6 ± 1.8
									Total fusion age = 121.8 Ma	

26 (6–20 μm) J = 0.004945 ± 0.5%; wt = 6.241 mg

500	161.24 ± 1.14	1.049 ± 0.018	0.012 ± 0.001	0.556 ± 0.057	0.5150 ± 0.0031	8.66	0.63	5.60	0.96	75.7 ± 31.2
525	14.88 ± 0.29	0.600 ± 0.006	0.003 ± 0.001	0.452 ± 0.046	0.0394 ± 0.0008	5.47	0.36	22.00	0.68	48.1 ± 4.1
550	8.99 ± 0.20	0.475 ± 0.006	0.003 ± 0.001	0.258 ± 0.040	0.0210 ± 0.0007	5.88	0.29	31.10	0.94	51.7 ± 2.9
575	10.58 ± 0.21	0.599 ± 0.006	0.002 ± 0.001	0.261 ± 0.044	0.0237 ± 0.0008	5.98	0.36	33.90	1.17	52.6 ± 2.4
600	12.04 ± 0.23	0.693 ± 0.007	0.003 ± 0.001	0.449 ± 0.049	0.0269 ± 0.0008	5.94	0.42	34.20	0.79	52.2 ± 2.3
625	14.01 ± 0.26	0.772 ± 0.007	0.002 ± 0.001	0.410 ± 0.049	0.0311 ± 0.0008	6.27	0.46	34.50	0.96	55.0 ± 2.9
650	15.56 ± 0.25	0.845 ± 0.011	0.004 ± 0.001	0.227 ± 0.052	0.0346 ± 0.0008	6.32	0.51	34.30	1.90	55.5 ± 3.3
675	10.08 ± 0.21	0.701 ± 0.006	0.003 ± 0.000	0.268 ± 0.046	0.0220 ± 0.0007	5.11	0.42	35.60	1.33	45.1 ± 1.9
700	9.20 ± 0.19	1.198 ± 0.007	0.002 ± 0.000	0.142 ± 0.040	0.0089 ± 0.0006	5.48	0.72	71.40	4.30	48.3 ± 0.7
750	22.76 ± 0.24	3.668 ± 0.020	0.004 ± 0.001	0.148 ± 0.056	0.0054 ± 0.0008	5.77	2.21	93.00	12.68	50.7 ± 0.6
800	52.37 ± 0.30	8.448 ± 0.022	0.014 ± 0.001	0.357 ± 0.052	0.0065 ± 0.0008	5.97	5.08	96.30	12.07	52.5 ± 0.4
850	124.84 ± 0.88	19.430 ± 0.089	0.016 ± 0.001	0.223 ± 0.058	0.0109 ± 0.0008	6.25	11.69	97.40	44.45	54.9 ± 0.6
900	223.51 ± 1.15	32.164 ± 0.132	0.022 ± 0.001	0.060 ± 0.071	0.0147 ± 0.0008	6.81	19.34	98.00	273.59	59.7 ± 0.6
950	268.67 ± 0.93	33.646 ± 0.112	0.032 ± 0.002	0.000 ± 0.000	0.0156 ± 0.0008	7.84	20.23	98.30	0.00	68.6 ± 0.5
1000	245.58 ± 0.76	24.858 ± 0.042	0.025 ± 0.002	0.019 ± 0.078	0.0122 ± 0.0008	9.73	14.95	98.50	673.45	84.8 ± 0.5
1050	190.15 ± 1.16	14.882 ± 0.039	0.023 ± 0.001	0.000 ± 0.000	0.0078 ± 0.0007	12.62	8.95	98.80	0.00	109.2 ± 0.8
1100	168.84 ± 0.73	11.289 ± 0.034	0.009 ± 0.001	0.010 ± 0.036	0.0071 ± 0.0008	14.76	6.79	98.70	556.79	127.1 ± 0.9
1200	187.86 ± 0.79	9.343 ± 0.046	0.013 ± 0.001	0.067 ± 0.060	0.0103 ± 0.0008	19.77	5.62	98.40	71.04	168.3 ± 1.3
1350	29.84 ± 0.29	1.315 ± 0.008	0.002 ± 0.001	0.009 ± 0.043	0.0038 ± 0.0008	20.72	0.79	91.30	72.42	176.0 ± 2.1
1650	10.16 ± 0.22	0.304 ± 0.005	0.004 ± 0.001	0.106 ± 0.045	0.0212 ± 0.0008	12.78	0.18	38.30	1.46	110.5 ± 3.2
									Total fusion age = 79.5 Ma	

33(6–20 μm)J = 0.00494 ± 0.5%; wt = 5.144 mg

500	117.93 ± 0.93	0.659 ± 0.015	0.020 ± 0.001	2.230 ± 0.095	0.3813 ± 0.0018	8.22	0.62	4.60	0.15	71.9 ± 37.1
525	16.26 ± 0.16	0.473 ± 0.007	0.011 ± 0.000	1.804 ± 0.063	0.0444 ± 0.0003	6.93	0.44	20.10	0.13	60.8 ± 5.6
550	10.87 ± 0.12	0.404 ± 0.005	0.010 ± 0.000	1.949 ± 0.064	0.0300 ± 0.0002	5.35	0.38	19.80	0.11	47.1 ± 4.3

Table 1 (Contd.)

T (°C)	^{40}Ar $\times 10^{-14}$moles	^{39}Ar $\times 10^{-14}$ moles	^{38}Ar $\times 10^{-14}$ moles	^{37}Ar $\times 10^{-14}$ moles	^{36}Ar $\times 10^{-14}$ moles	$^{40}Ar^a/^{39}Ar$	$\%^{39}Ar_K$	$\%^{40}Ar^a$	K/Ca	Age $\pm 2\sigma$
33(6–20 μm)J = 0.00494 ± 0.5%; wt = 5.144 mg										
575	16.71 ± 0.22	0.641 ± 0.007	0.011 ± 0.000	2.087 ± 0.072	0.0424 ± 0.0004	6.80	0.60	26.00	0.16	59.6 ± 5.2
600	15.70 ± 0.11	0.477 ± 0.004	0.011 ± 0.000	1.752 ± 0.074	0.0428 ± 0.0003	6.68	0.45	20.20	0.14	58.5 ± 4.5
625	13.87 ± 0.09	0.435 ± 0.002	0.009 ± 0.000	1.377 ± 0.060	0.0369 ± 0.0002	7.07	0.41	22.10	0.16	61.9 ± 3.4
650	14.12 ± 0.18	0.631 ± 0.008	0.012 ± 0.000	2.109 ± 0.070	0.0343 ± 0.0003	6.58	0.59	29.30	0.15	57.7 ± 4.6
675	8.14 ± 0.08	0.511 ± 0.004	0.009 ± 0.000	1.889 ± 0.066	0.0187 ± 0.0003	5.40	0.48	33.80	0.14	47.5 ± 2.6
700	9.34 ± 0.08	0.982 ± 0.005	0.009 ± 0.000	1.649 ± 0.061	0.0138 ± 0.0002	5.50	0.92	57.80	0.30	48.3 ± 0.9
750	17.71 ± 0.09	2.236 ± 0.013	0.012 ± 0.001	1.491 ± 0.056	0.0119 ± 0.0002	6.40	2.09	80.90	0.76	56.2 ± 0.7
800	38.83 ± 0.19	6.125 ± 0.019	0.015 ± 0.001	1.638 ± 0.062	0.0121 ± 0.0002	5.77	5.73	91.10	1.91	50.7 ± 0.5
850	82.72 ± 0.34	12.691 ± 0.039	0.024 ± 0.001	1.115 ± 0.056	0.0148 ± 0.0002	6.17	11.88	94.80	5.81	54.2 ± 0.5
900	145.80 ± 0.81	18.158 ± 0.061	0.031 ± 0.002	0.793 ± 0.050	0.0186 ± 0.0002	7.72	16.99	96.20	11.68	67.5 ± 0.5
950	184.94 ± 0.84	21.565 ± 0.089	0.033 ± 0.002	0.804 ± 0.050	0.0181 ± 0.0002	8.32	20.18	97.10	13.68	72.7 ± 0.6
1000	158.59 ± 0.53	15.805 ± 0.063	0.031 ± 0.002	0.711 ± 0.050	0.0113 ± 0.0002	9.82	14.79	97.90	11.34	85.5 ± 0.7
1050	139.71 ± 0.57	11.088 ± 0.029	0.020 ± 0.001	0.652 ± 0.054	0.0079 ± 0.0002	12.39	10.38	98.40	8.68	107.2 ± 0.7
1100	121.54 ± 0.62	7.857 ± 0.035	0.014 ± 0.000	0.642 ± 0.050	0.0073 ± 0.0002	15.19	7.35	98.20	6.24	130.6 ± 1.2
1200	123.90 ± 0.20	5.335 ± 0.010	0.006 ± 0.000	0.627 ± 0.051	0.0086 ± 0.0002	22.76	4.99	98.00	4.34	192.2 ± 0.9
1350	12.41 ± 0.06	0.510 ± 0.002	0.005 ± 0.000	0.694 ± 0.053	0.0050 ± 0.0002	21.57	0.48	88.60	0.38	182.7 ± 1.1
1650	7.70 ± 0.07	0.272 ± 0.002	0.007 ± 0.000	0.903 ± 0.062	0.0148 ± 0.0002	12.50	0.25	44.10	0.15	108.1 ± 2.3
									Total fusion age = 83.3 Ma	

[a] Ar = radiogenic argon; $^{39}Ar_K$ = neutron induced ^{39}Ar produced from ^{39}K

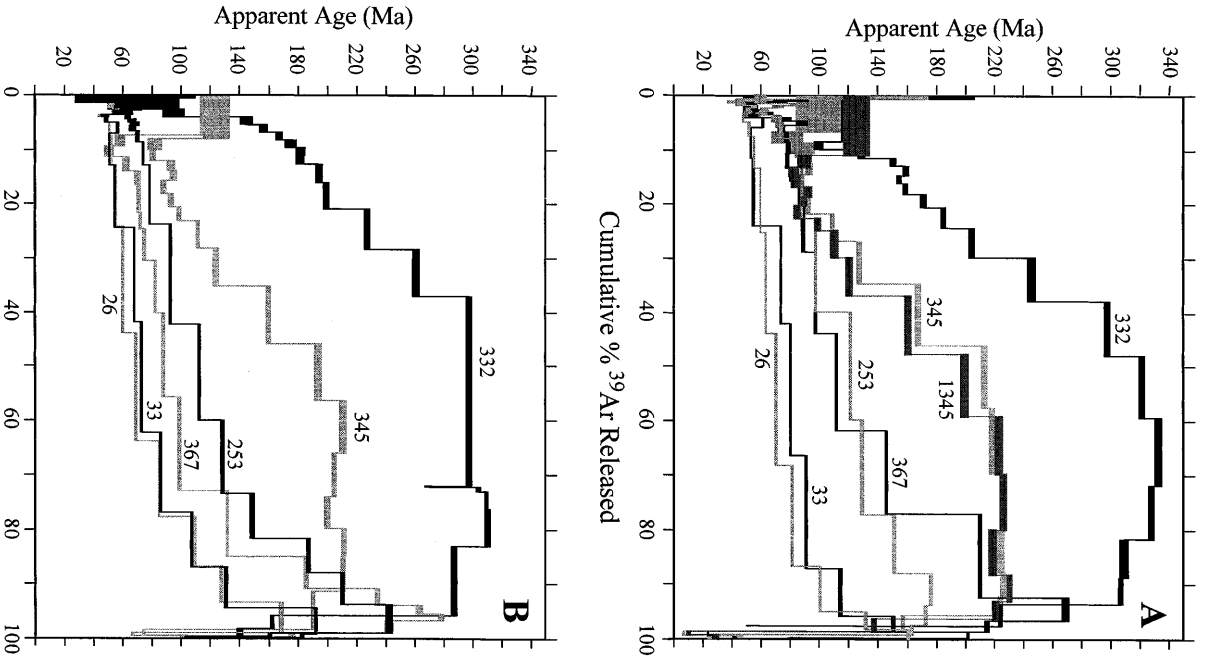

Fig. 3 **a** $^{40}Ar/^{39}Ar$ spectra for the 2–6 μm size fractions. Sample *numbers* are indicated **b** $^{40}Ar/^{39}Ar$ spectra for the 6–20 μm size fractions. Sample *numbers* are indicated

physical and chemical properties of the analyzed material (Weaver et al. 1984; Wijbrans and McDougall 1986; Hassanipak and Wampler 1996). The amount of ^{40}Ar and ^{39}Ar released is strongly controlled by the degree of metamorphism of the sample and is more or less independent of the size fraction, which means that it is most strongly dependent on the degree of illitization. This behavior is shown in Fig. 4, where the % ^{40}Ar released from the 2–6 μm size fraction is plotted against temperature. The least metamorphosed samples release argon at significantly lower temperatures than the more metamorphosed samples, and release argon over a

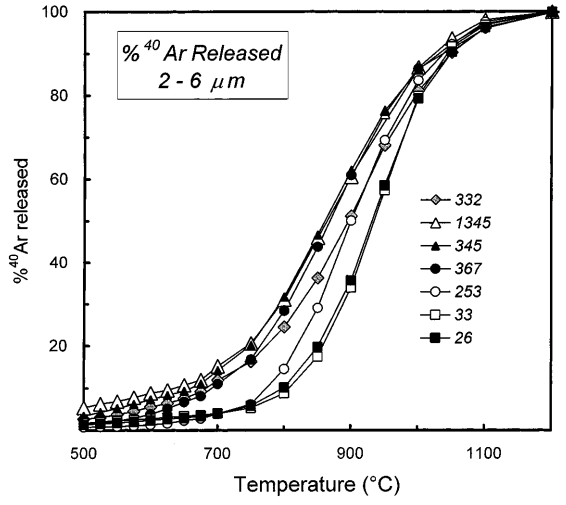

Fig. 4 Plot of temperature versus ^{40}Ar released for the 2–6 μm samples. Note the more restricted temperature range over which the phyllosilicates degas as metamorphism proceeds

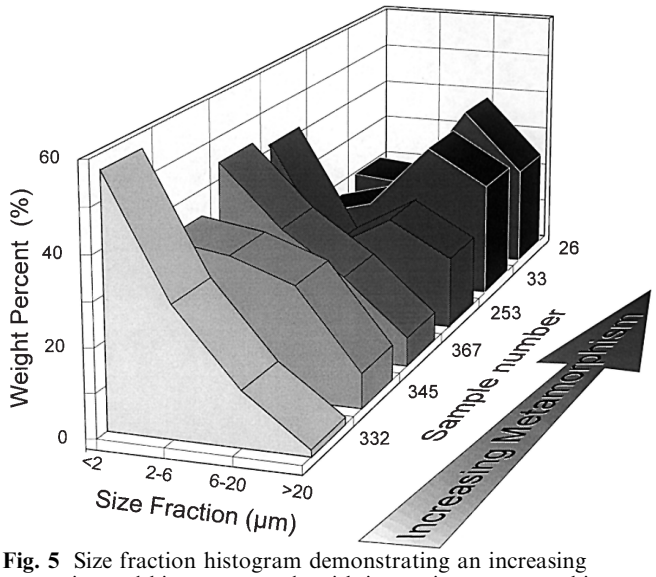

Fig. 5 Size fraction histogram demonstrating an increasing mean size and histogram mode with increasing metamorphism. Note the bimodal distribution in particle size in sample 253 and the evolution to coarser particle sizes in the more highly metamorphosed samples (26 and 33)

broader range of temperatures between 500 and 1100 °C. In contrast, the more metamorphic samples release the majority of argon within a narrow temperature interval, between about 750 and 1000 °C.

The presence of chlorite has no noticeable effect on the apparent ages of the samples analyzed. Samples 26 and 33, which represent the most metamorphosed samples, display nearly identical behavior with respect to their argon degassing patterns, yet sample 33 contains noticeable chlorite (Fig. 2b). The sample not treated by saturation with $MgCl_2$ degasses at slightly lower temperatures and has a slightly younger $^{40}Ar/^{39}Ar$ total fusion age (~2 Ma). Because of the slight shift in the degassing pattern it perhaps indicates that, in samples containing mixed-layer illite/smectite, some loosely bound K atoms may be exchanged with Mg in the interlayer site leading to slightly lower $^{40}Ar/^{39}Ar$ ratios, and therefore younger apparent ages, in the non-treated samples.

Evolution of sample particle size and morphology

A histogram illustrating the weight percent variation in the different size fractions of the separated insoluble minerals, including quartz and albite, is shown in Fig. 5. The three least metamorphosed samples (332, 345, 367) contain a much higher percentage of small particles (< 2 μm) than the more metamorphic samples. In addition, these samples display a regular, decreasing relationship in the abundance of particles with increasing size. In contrast, an abrupt change occurs between samples 367 and 253, as there is no longer a regular decrease in sample size but a significant appearance of particles in the size range 6–20 μm.

The progressive change in morphology of the sample particles viewed by scanning electron microscopy is shown in Figs. 6 and 7. The least metamorphosed sample (332) shows a heterogeneous distribution of phyllosilicates, quartz and albite. With increasing metamorphism the amounts of quartz and albite decrease (Fig. 6), however, the XRD powder diffractograms indicate detectable amounts remain in all samples. In the least metamorphosed samples the phyllosilicates typically occur as aggregates or flakes, which are rounded yet display irregular edges at high magnification (Fig. 7a). With increased metamorphism the phyllosilicates are thin, sharp edged plates, some with well-developed crystallographic faces often exhibiting evidence of overgrowths and/or dissolution (Fig. 6).

XRD data and decomposition with Newmod©: results and interpretation

The X-ray diffractograms from the oriented ethylene glycol exchanged preparations of the 2–6 μm size fraction have been modeled from the sum of Newmod© (Reynolds 1985; Reynolds and Reynolds 1996) simulations. This technique permits a distinction between detrital mica and neoformed illite/smectite. This decomposition technique is slightly different than that used by Lanson and Besson (1992), who also modeled a detrital component. Samples 332, 345, 367 and 253 display an unambiguous relationship between metamorphic grade and illite content in the mixed-layer illite/smectite, which progressively increases from 65% to ~97% (Table 2, Fig. 2a and 6). This increased illite content in the illite/smectite is interpreted as directly related to progressive neoformation of illite. Moreover, evolution is accompanied by increased thickness of the coherent diffraction domains as shown by many authors

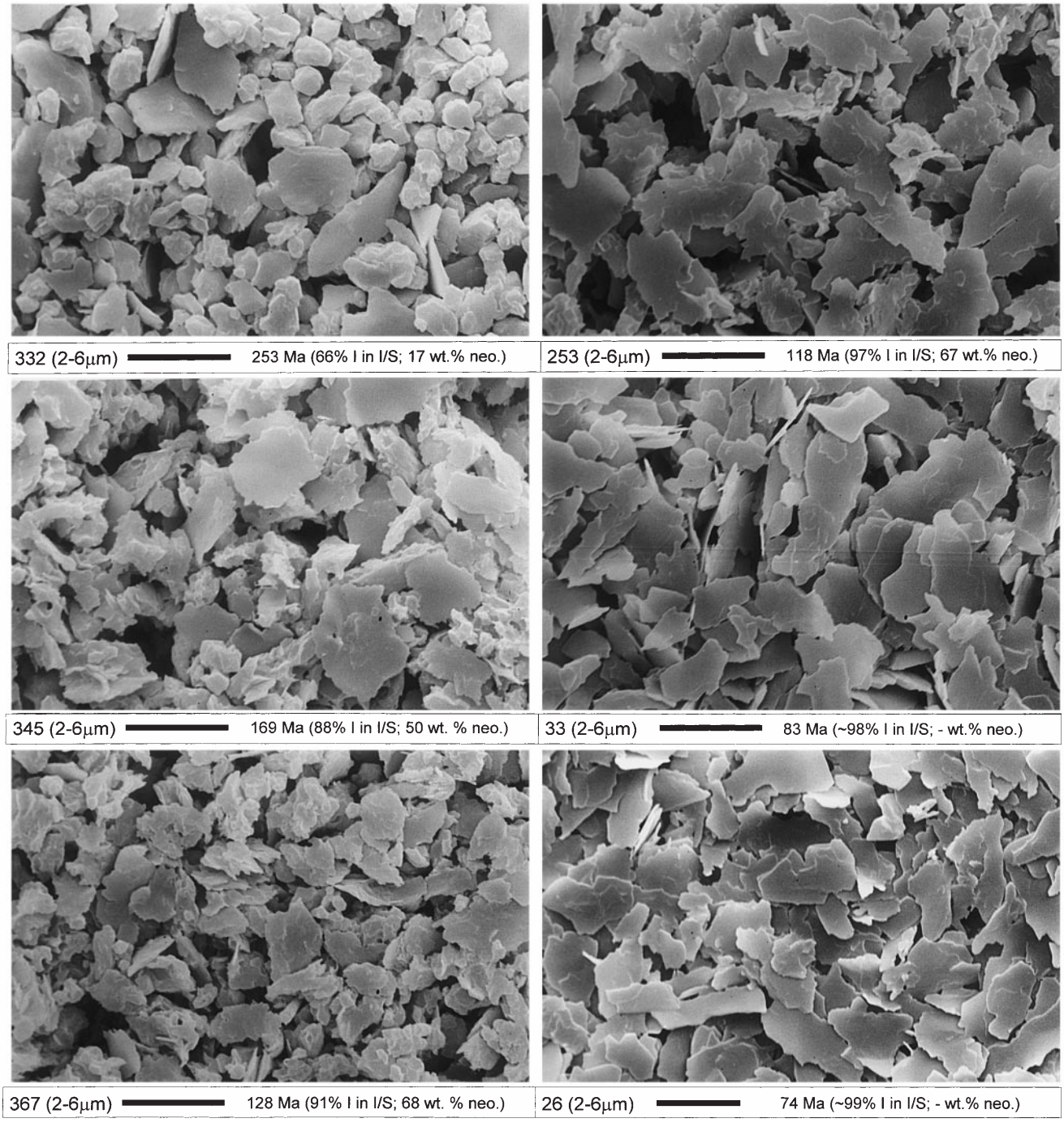

Fig. 6 SEM photographs of the 2–6 μm size fractions. Note the progressive change in phyllosilicate morphology, whereby samples become more homogeneous and contain fewer aggregates with increasing metamorphism. Also note the presence of similarly sized grains of (neoformed?) quartz and albite that become less abundant with increasing metamorphism. *Black scale bar* is 10 μm in all photographs

(Peacor 1992: Pollastro 1993; Whitney and Velde 1993; Jaboyedoff and Thélin 1996; Altaner and Ylgang 1997; Moore and Reynolds 1997). For the most strongly metamorphosed samples (26 and 33) the illite content in the illite/smectite is such (>97% I) that it is impossible to distinguish between a mixed-layer illite/smectite and true mica. Sample 253, which occurs at the transition from diagenesis to anchizone, defines the passage from illite/smectite to a "mica-like" composition. This sample also marks a significant change from small to larger particle sizes (Fig. 5).

Two methods are possible to quantify the proportion of neoformed illite layer in a sample. One is to compute the ratio of the weight percent (wt%) of the illite layers in the illite/smectite over the sum of the wt% of the illite layers in the illite/smectite plus mica. However, this result only considers the illite layer and does not consider

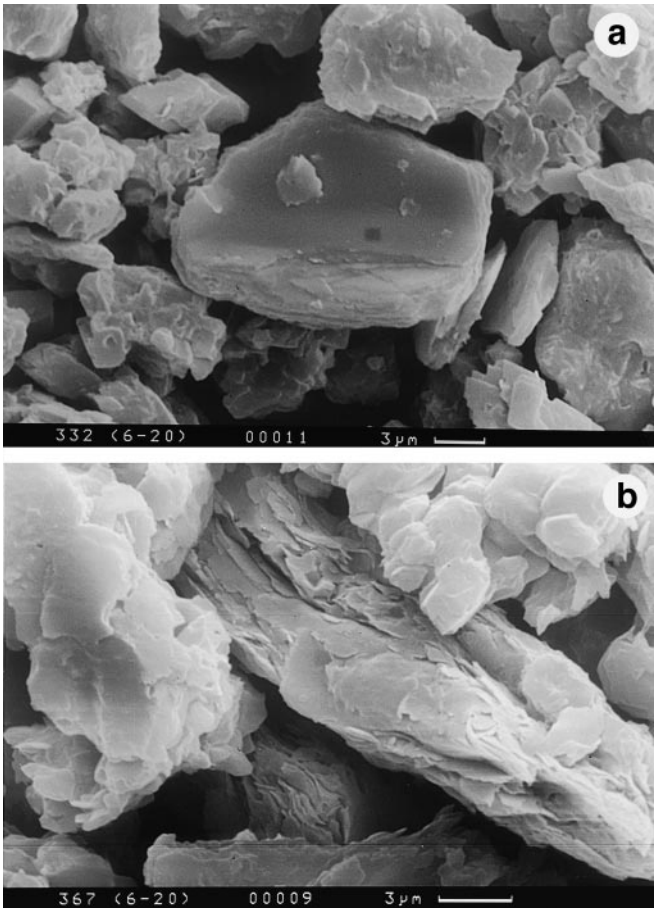

Fig. 7a,b SEM photographs of: **a** detrital mica in the 6–20 µm size fraction from the least metamorphic sample (332); **b** "Rose"-shaped illite/smectite aggregate observed in the 6–20 µm size fraction of sample 367. This "rose" morphology demonstrates that a size fraction is not only composed of discrete grains but also of aggregates subdivided into grains and subgrains

the possible presence of smectite. Therefore, a second method normalizing the results calculated as above to the total amount of mica and illite/smectite, including the wt% of smectite layer in the total, such that when the sum of illite layer plus mica = 100% the amount of smectite layer is zero (Table 2).

Significance of ages from mixtures of dioctahedral phyllosilicates

From the results presented above it is clear that the samples contain variable mixtures of detrital dioctahedral mica (= pure dioctahedral mica in the simulation) and mixed-layer illite/smectite containing variable amounts of illite layers (< 100% I). For the most highly metamorphosed samples the illite in the mixed layers is indistinguishable from true mica. The $^{40}Ar/^{39}Ar$ apparent ages from these mixtures (Fig. 3) most probably reflect various contributions from neoformed grains or subgrains formed during the low-grade Alpine metamorphic event together with detrital muscovites and/or phengites derived from the erosion of Permian–Carboniferous granitic rocks (Frey et al. 1976). However, as micas entirely of detrital origin may have undergone structural modifications during transport, deposition, and/or early diagenesis (Kübler 1984), they may not be expected to yield simple $^{40}Ar/^{39}Ar$ age spectra. The weakness of some $2M_1$ reflections may indicate some lattice defects. Such defects could lead to poorly retentive sites for argon and may be expected to yield younger $^{40}Ar/^{39}Ar$ ages than Permian at low laboratory temperatures (see also Dallmeyer and Neubauer 1994). The age of the illite layer in the illite/smectite can be viewed as a continuum, reflecting the time interval over which neoformation occurred (Kirschner et al. 1996).

The apparent $^{40}Ar/^{39}Ar$ total fusion ages of all samples decrease as the amount of the illite layers in the mixed-layer illite/smectite increase (Fig. 8). This relation can be used to identify end-members of mixtures consisting of detrital and neoformed mica and illite layers. Figure 9 is a plot of $^{40}Ar/^{39}Ar$ total fusion age versus the % neoformed illite content for the four least metamorphic samples, using the two methods described above. As the curve fitting the data very nearly approaches a linear relationship (Fig. 9), a linear fit has been used for simplicity to obtain end-members. For the first method ignoring smectite, a linear regression ($R^2 = 0.992$) yields intercepts with 2σ errors of 38^{+30}_{-54} and 300^{+55}_{-30} Ma for 100% neoformed and 100% detrital mica, respectively. A linear regression using the second method considering smectite results in a more precise fit ($R^2 = 0.999$) with intercepts at 27^{+11}_{-14} Ma and 295^{+10}_{-10} Ma. A mixing curve calculated with these end-member ages agrees well with fit obtained by the regression method (Fig. 9). These end-member ages are also consistent with both geological and biostratigraphic constraints for the low-grade Alpine metamorphism of these rocks and the source rock age for the detrital grains (Frey et al. 1976; Caron et al. 1989; Badoux 1996; Escher et al. 1997; Burkhard and Sommaruga in press). The simulated X-ray diffraction data for the < 2 µm fractions (see Jaboyedoff and Thélin 1996) for which no age data are currently available show a similar trend in the percentage of neoformed illite.

Model

In order to test the validity of the interpretation of a mixture of neoformed illite layers of Tertiary age together with detrital dioctahedral mica of Permo-Carboniferous age, simulations of such mixtures have been calculated (Fig. 10). Model $^{40}Ar/^{39}Ar$ age spectra have been calculated (Fig. 10) using a contribution of neoformed illite formed at 27 Ma together with detrital dioctahedral mica of variable age in order to replicate the measured argon release characteristics (Fig. 4) and $^{40}Ar/^{39}Ar$ spectra (Fig. 3) for the 2–6 µm size fractions. For these calcula-

Table 2 XRD simulation results. Minerals in italics are assumed to be of detrital origin (*Dimica* dioctahedral mica, *I/S* illite/smectite, *2gly* 2 layer ethylene glycol)

Sample	Mineral	%Illite layer in I/S	Total %dimica or illite layer in I/S	Layer number range	Defect free distance	R(Reichweite) and remarks	Wt%	Wt% (illite neoformed)/(total Mica + I/S)	Wt% (illite neoformed)/(total mica + illite in I/S)
332	Glycolated								
	I/S-2gly	60%		2–12		0.5	11%		
			66%					15%	17%
	I/S-2gly	70%		2–14		1	14%		
	Dimica	100%		2–14			28%		
	Dimica	100%	100%	1–70	21		43%	75%	83%
	Dimica	100%		25–35			3%		
	Pyrophylite			2–14					
345	Glycolated								
	I/S-2gly	80%		2–14		0.5	11%		
	I/S-2gly	85%	88%	5–20		1	16%	46%	50%
	I/S-2gly	93%		7–25		1	27%		
	Dimica	100%		1–70	30		22%		
	Dimica	100%	100%	5–20			16%	46%	50%
	Dimica	100%		1–100	70	$d = 9.94$ Å	8%		
367	Glycolated								
	I/S-2gly	90%		8–20		1	52%		
			91%					63%	68%
	I/S-2gly	95%		25–35		1	18%		
	Dimica	100%		1–70	30		5%		
	Dimica	100%	100%	5–20			16%	30%	32%
	Dimica	100%		1–100	70	$d = 9.94$ Å	9%		
253	Glycolated								
	I/S-2gly	97%		5–25		1	42%		
			97%					66%	67%
	I/S-2gly	98%		20–40		1	26%		
	Dimica	100%	100%	1–100	45		32%	32%	33%
33	Glycolated								
	I/S-2gly	97%		50–70	di = 9.95A	1	19%		
	I/S-2gly	99%	99%	20–40		1	37%	73%	74%
	I/S-2gly	99%		60–80	di = 9.95A	1	19%		
	Dimica	100%	100%	1–100	70	$d = 9.94$ Å	25%	26%	26%
26	Glycolated								
	I/S-2gly	97%		50–70	di = 9.95A	1	31%		
	I/S-2gly	99%	99%	60–70	di = 9.95A	1	26%	90%	92%
	I/S-2gly	99%		20–40		1	36%		
	Dimica	100%		60–80		$d = 9.94$ Å	5%		
			100%					8%	8%
	Dimica	100%		1–100	70	$d = 9.94$ Å	3%		

tions only ratios of detrital mica and illite layers are considered. The neoformed illite layers are assumed to have a constant age of 27 Ma and the detrital micas are assumed to have maximum ages between 295 Ma and 330 Ma, which is consistent with what is observed in the measured $^{40}Ar/^{39}Ar$ spectra (Fig. 3). Small differences in the age of the detrital input are taken into consideration, because detrital mica can also be considered a mixture and thus the age of the detrital mica can not be assumed constant. For these calculations the detrital component is assumed to become slightly younger with increasing metamorphism. In any case small differences in the maximum age of the detrital input have little influence on the modeled results. The results of the model calculations indicate that excellent agreement can be obtained between the measured and calculated $^{40}Ar/^{39}Ar$ spectra with mixtures of neoformed illite layers and detrital micas (Fig. 10). Moreover, the results of the model calculations underscore two important empirical observations. First, the range of temperatures over which ^{40}Ar is released from the detrital population becomes more restricted with increasing metamorphism (Weaver et al. 1984). Second, with increasing metamorphism the neoformed illite layers degas at progressively higher temperatures, and samples from the highest metamorphic grade degas at temperatures similar to those for detrital micas.

Discussion

By investigating a single stratigraphic unit subjected to varying degrees of low-grade metamorphism it is possible to focus on systematic changes in both mineralogy and argon geochemistry resulting from this metamorphism (Clauer et al. 1995). In the size fractions investigated, systematic changes of increased grain size, and

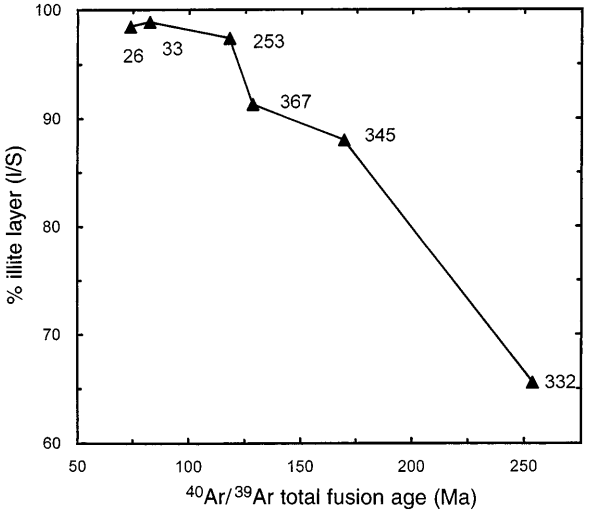

Fig. 8 Plot of total fusion $^{40}Ar/^{39}Ar$ age versus the % illite layer in the illite/smectite of the 2–6 μm size fraction. All illite is considered to be neoformed. This relationship is non-linear because such a plot does not consider the contribution of detrital mica or the wt% of the neoformed illite layer

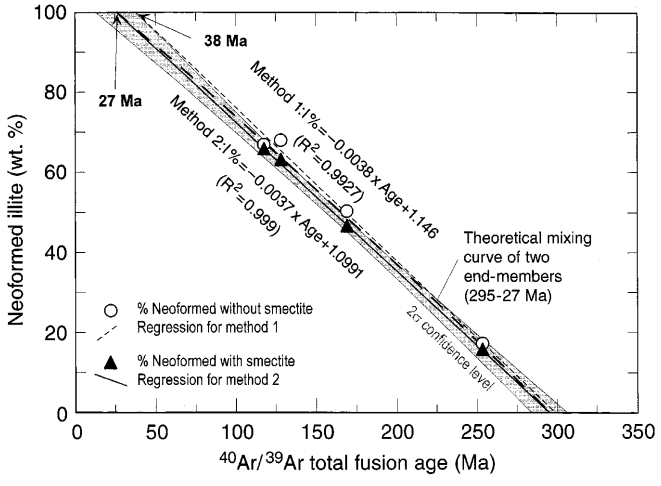

Fig. 9 Plot of total fusion $^{40}Ar/^{39}Ar$ age versus the wt% of neoformed illite layer. This plot takes into consideration both detrital mica and neoformed illite layers. Regression methods 1 and 2 are described in the text. The calculated mixing age curve for end-member ages of 27 and 295 Ma is also indicated

homogeneity in phyllosilicate morphology are observed and can directly be correlated to progressive metamorphism. The measured and model $^{40}Ar/^{39}Ar$ step-heating spectra, together with the X-ray diffraction data and SEM observations are consistent with these progressive changes in the mineralogy of the samples during prograde incipient metamorphism.

This study clearly indicates that with progressive metamorphism (from incipient to low-grade metamorphic conditions) detrital dioctahedral mica disappears and yields to neoformed illite layers. The detrital mica, perhaps partially destroyed during transport, may readily transform altered layers directly into neoformed mica. Evidence for this behavior is supported by the argon degassing properties of the detrital component in the modeled $^{40}Ar/^{39}Ar$ spectra (Fig. 10) in which detrital mica degasses over a progressively narrower temperature interval and becomes slightly younger with increased metamorphism. This could also be the result of a progressive dissolution of detrital mica, beginning with the smallest grains. The tendency toward a higher and restricted range of laboratory temperatures for the modeled release of argon from the neoformed illite layers in the illite/smectite is consistent with a progression toward phengite, probably of $2M_1$ polytype, with increasing (mid-anchizonal) metamorphism. From diagenesis to incipient metamorphism it is generally accepted that the 1M or $1M_d$ polytypes are the early neoformed illite and are generally replaced by the $2M_1$ polytype (Lanson and Besson 1992; Grathoff and Moore 1996; Moore and Reynolds 1997). However, this evolution is difficult to establish in the presence of weathered, detrital mica (Drits et al. 1993; Dalla Torre et al. 1994; Moore and Reynolds 1997).

The principal mechanism for neoformation of illite layers in the studied rocks remains unclear; however, the results provide the basis for some speculation. The appearance of neoformed mica-like layers and the disappearance of detrital mica, together with distinct morphological characteristics may be evidence for a process of dissolution and reprecipitation. Such an interpretation requires at least a process that is distinct from the conclusions of Hunziker et al. (1986), who invoked a process of "restructuration" without recrystallization in illites at similar metamorphic grades. They concluded on the basis of stable and radiogenic isotope data that ionic exchange in illites occurs along interlayer positions, but that the silicon-oxygen bonds remained intact. Our interpretation of short-range recrystallization makes no restrictions about the silicon-oxygen framework, which may remain intact but becomes repositioned during reprecipitation.

The reason for metastability of the detrital dioctahedral mica is not clear, but there are some data to indicate that the illite layer, which is compositionally distinct from phengite or muscovite (Meunier and Velde 1989; Srodon et al. 1992), may be easier to crystallize at low-grade metamorphic conditions. The morphology of the neoformed grains in the most metamorphic samples is clearly distinct from that of detrital grains, yet some record of older ages is preserved in these grains. This may indicate that some small detrital grains acted as nuclei for overgrowths of neoformed illite layers (Whitney and Velde 1993). This point is supported by the observation that cores of neoformed grains have, at a qualitative level determined from energy dispersive analysis with the SEM, similar concentrations of titanium to that of the detrital grains. In addition, the surface area and the ratio of the length over the width of the phyllosilicates may play a role in the stability of the detrital mica, such that preferential dissolution occurs in the smallest sizes and progresses more slowly with the

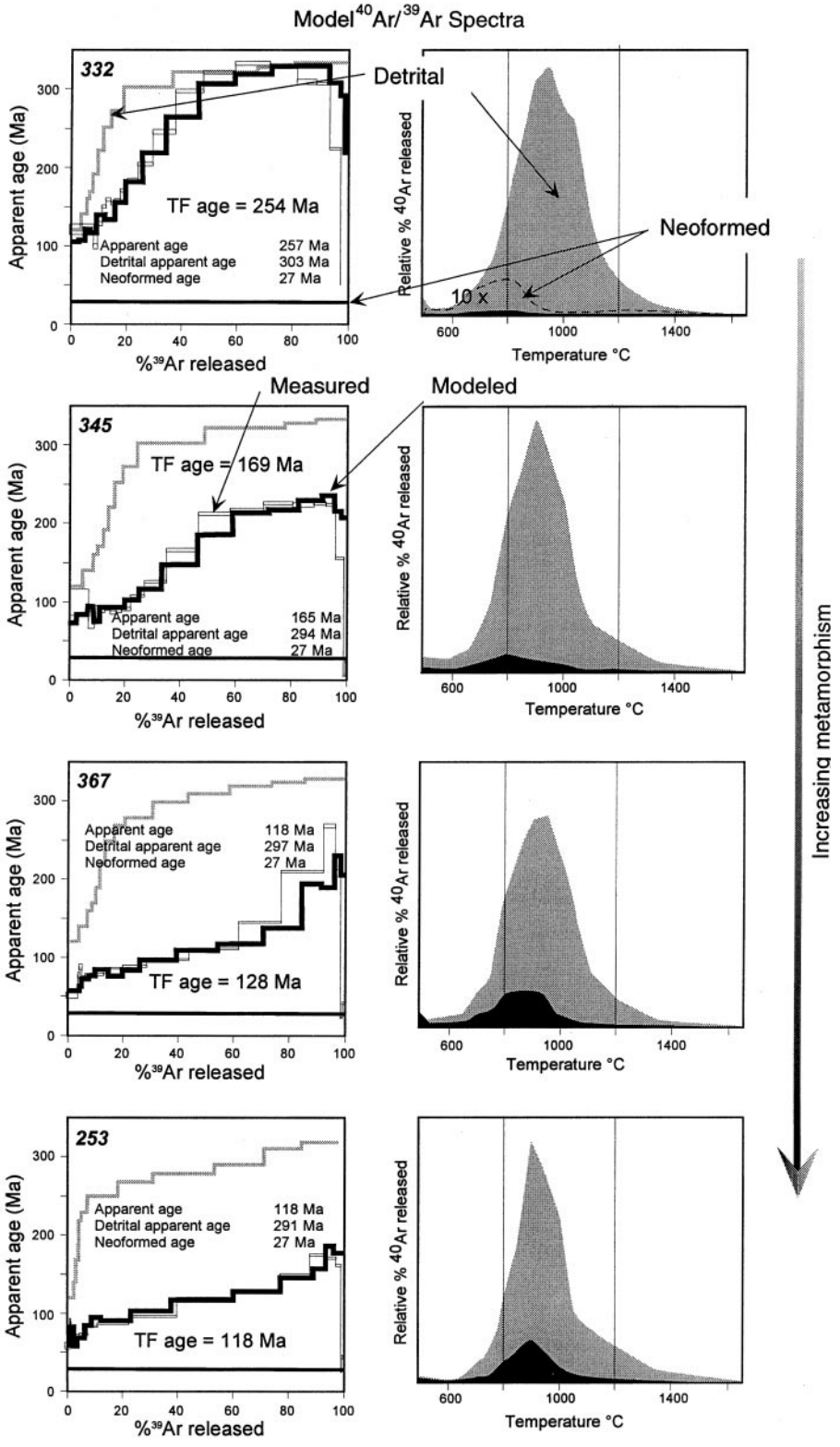

Fig. 10 Model $^{40}Ar/^{39}Ar$ spectra constructed from the proportion of neoformed illite and detrital mica layers obtained by Newmod© simulations together with the measured $^{40}Ar/^{39}Ar$ total fusion ages and % ^{39}Ar released. The model $^{40}Ar/^{39}Ar$ age spectra (*shown in bold*) are obtained assuming a 27 Ma age for the neoformed illite layers and variable, but very similar contributions of detrital mica. The *adjoining* plots illustrate the modeled amount of ^{40}Ar released, originating from the detrital and neoformed phyllosilicates (illite). Note the progressive increase in ^{40}Ar contributed by neoformed illite with increasing metamorphism. Note also that distinct laboratory degassing temperatures for detrital and neoformed grains are only observed at the lowest metamorphic grade and with increased metamorphism all phyllosilicates degas in a single, narrow temperature interval. These tendencies indicate a similar physical and chemical behavior of the neoformed illite and detrital mica at the highest metamorphic grade. The scale is given in relative $\%^{40}Ar$ released. The contribution of neoformed illite in sample 332 is magnified 10 times in order to illustrate its degassing temperature

largest detrital grains. Dissolution of detrital mica and precipitation of illite is an attractive explanation for the neoformation of some dioctahedral illite (Lanson and Meunier 1995) because it permits loss of argon from the micas. However, the process of dissolution and reprecipitation may occur in different steps, either as overgrowths on preexisting mica or on illite/smectite or through a series of intermediate steps involving precipitation of mixed-layer illite/smectite, solid state transformation or short range recrystallization (Altaner and Ylgang 1997; Moore and Reynolds 1997). The probable metastability of illite does not change the previous dis-

cussion (Essene and Peacor 1995, 1997). It is also possible to have some neoformed mica layers within detrital micas that have undergone some alteration during transport and early diagenesis or to have illite/smectite with a detrital origin. However, these are small effects and X-ray diffraction techniques can generally distinguish such contributions (Pevear 1992).

Concluding remarks

The extrapolated age of 27 Ma for the case of 100% neoformed illite, which is interpreted as the age of incipient metamorphism of the Couches Rouges stratigraphic unit, agrees well with geological evidence. Tectonic burial of the Préalpes Médianes began around 47–40 Ma and thrusting onto the Molasse occurred at least until ~25 Ma. Moreover, these results are consistent with the data of De Coulon (1990), who reported K/Ar ages of ~60 Ma for the < 2 μm size fractions of white mica from the Amselgrat klippe, which represents the same stratigraphic unit but subjected to slightly greater metamorphic conditions than samples 26 and 33 of this study. These results can also be interpreted as mixtures of detrital and neoformed phyllosilicates, with the increased metamorphic conditions from the Amselgrat being reflected in the younger total fusion ages.

Combining $^{40}Ar/^{39}Ar$ dating with X-ray diffraction modeling techniques in low-grade metamorphic rocks provides a useful tool for the timing of neoformation and metamorphism of suitable samples up to conditions of the diagenesis-anchizone transition. Beyond this limit it is not possible to distinguish between neoformed mixed-layer illite/smectite and detrital mica using conventional X-ray techniques. Moreover, at metamorphic conditions above anchizone the degassing properties of the detrital and neoformed grains converge and a two component mixture may yield a $^{40}Ar/^{39}Ar$ plateau age of no geological significance. However, for many rocks metamorphosed at conditions of diagenesis to anchizone, such as basinal settings where there is a measurable increase in metamorphism with depth, this technique should be widely applicable.

Acknowledgements This investigation has been supported by the Swiss National Science Foundation (project numbers 21-26433.89, 20-31234.91, 2000-0505311.97). We wish to thank P. Thélin, A. Escher, M. Sartori, and A. Baud for support, discussion and encouragement. Many discussions with J. Hunziker and B. Kübler on the isotopic dating of low-grade minerals and with F. Bussy, J.L. Epard, H. Masson, J. Mosar and G. Stampfli on the geological significance of our data helped us to refine many of the ideas presented. Comments and reviews by N. Clauer, E. Essene, and M. Frey are gratefully acknowledged.

References

Altaner SP (1989) Calculation of K diffusional rates in bentonite beds. Geochim Cosmochim Acta 53: 923–931

Altaner SP, Ylgang RF (1997) Comparison of structural models of mixed-layer illite/smectite and reaction mechanisms of smectite illitization. Clays Clay Miner 45: 517–533

Aronson JL, Hower J (1976) Mechanism of burial metamorphism of argillaceous sediment. II. Radiogenic argon evidence. Geol Soc Am Bull 87: 738–744

Badoux H (1996) Le substratum des Préalpes du Chablais. Bull Soc Vaudoise Sci Nat 84: 113–124

Barnes DA, Girard JP, Aronson JL (1992) K-Ar dating of illite diagenesis in the middle Ordovician St. Peter sandstone, central Michigan Basin, USA: implication for thermal history. In: Houseknecht DW, Pittmann ED (eds) Origin, diagenesis, and petrophysics of clay minerals in sandstones. Soc Econ Paleontol Mineral Spec Publ: 35–48

Baud A (1987) Stratigraphie et sédimentologie des calcaires de St-Triphon. Mem Geol Lausanne: 1

Baud A, Septfontaine M (1980) Présentation d'un profil palinspastique de la nappe des Préalpes Médianes en Suisse occidentale. Eclogae Geol Helv 73: 651–660

Bonhomme MG, Dos Santos RP, Renac C (1995) La datation potassium-argon des minéraux argileux: etat des connaisances. Bull Centr Rech Explor Prod 19: 197–223

Brockamp O, Clauer N, Zuther M (1994) K-Ar dating of episodic Mesozoic fluid migrations along the fault system of Gernsbach between the Moldanubian and Saxothuringian (northern Black Forest, Germany). Geol Rundsch 83: 180–185

Burkhard M, Sommaruga A (1998) Evolution of the western Swiss molasse basin: structural relations with the Alps and the Jura belt. In: Merle, et al (eds) Spec Publ Geol Soc, London (in press)

Caron C, Homewood P, Wildi W (1989) The original Swiss flysch; a reappraisal of the type deposits in the Swiss Prealps. Earth-Sci Rev 26: 1–45

Clauer N, Chaudhuri S (1995) Inter-basinal comparison of diagenetic evolution of illite/smectite minerals in buried shales on the basis of K-Ar systematics. Clays Clay Miner 44: 818–824

Clauer N, Chaudhuri S, Kralik M, Bonnot-Courtois C (1993) Effects of experimental leaching on Rb-Sr and K-Ar isotopic systems and REE contents of diagenetic illite. Chem Geol 103: 1–4

Clauer N, Rais N, Schaltegger U, Pique A (1995) K-Ar systematics of clay-to-mica minerals in a multi-stage low-grade metamorphic evolution. Chem Geol 124: 3–4

Clauer N, Srodon J, Francu J, Sucha V (1997) K-Ar dating of illite fundamental particles separated from illite-smectite. Clay Miner 32: 181–196

Cosca MA, Hunziker JC, Huon S, Masson H (1992) Radiometric age constraints on mineral growth, metamorphism, and tectonism of the Gummfluh klippe, Briançonnais domain of the Préalpes, Switzerland. Contrib Mineral Petrol 112: 439–449

Cosca MA, Mezger K, Essene EJ (1998) The Baltica-Laurentia connection: Sveconorwegian (Grenvillian) metamorphism, cooling, and unroofing in the Bamble Sector, Norway. J Geol 106: 539–552

Dalla Torre M, Stern WB, Frey M (1994) Determination of white K-mica polytype ratios: comparison of different XRD methods. Clay Miner 29: 717–726

Dallmeyer RD, Neubauer F (1994) Cadomian $^{40}Ar/^{39}Ar$ apparent age spectra of detrital muscovites from the Eastern Alps. J Geol Soc London 151: 591–598

Dalrymple GB, Alexander EC, Lanphere MA, Kraker GP (1981) Irradiation of samples for $^{40}Ar/^{39}Ar$ dating using the Geological Survey TRIGA reactor. US Geol Surv Prof Pap 1176

De Coulon S (1990) Géologie et mineralogie de l'écaille de l'Amselgrat (unpublished). Diplome thesis, Univ Lausanne

Dong H, Hall CM, Halliday AN, Peacor DR, Merriman RJ, Roberts B (1997) $^{40}Ar/^{39}Ar$ illite dating of late Caledonian (Acadian) metamorphism and cooling of K-bentonites and slates from the Welsh Basin, U.K.. Earth Planet Sci Lett 150: 337–351

Drits VA, Weber F, Salyn AL, Tsipursky SI (1993) X-ray identification of one-layer illite varieties: application to the study of illites around uranium deposits of Canada. Clays Clay Miner 41: 389–398

Drits VA, Sakharov BA, Lindgreen H, Salyn A (1997) Sequential structure transformation of illite-smectite-vermiculite during diagenesis of Upper Jurassic shales from the North Sea and Denmark. Clay Miner 32: 351–371

Epard JL, Escher A (1996) Transition from basement to cover: a geometric model. J Struct Geol 18: 533–548

Escher A, Hunziker JC, Marthaler M, Masson H, Sartori M, Steck A (1997) Geologic framework and structural evolution of the Western Swiss-Italian Alps. In: Pfiffner OA, Lehner P, Heitzmann P, Mueller S, Steck A (eds) Deep structure of the Swiss Alps (results of the NRP 20). Birkhäuser, pp 205–221

Essene EJ, Peacor DR (1995) Clay mineral thermometry; a critical perspective. Clays Clay Miner 43: 540–553

Essene EJ, Peacor DR (1997) Illite and smectite; metastable, stable or unstable? Further discussion and a correction; reply. Clays Clay Miner 45: 116–122

Frey M, Hunziker JC, O'Neil JR, Schwander HW (1976) Equilibrium-disequilibrium relations in the Monte Rosa granite, western Alps: petrological, Rb-Sr and stable isotope data. Contrib Mineral Petrol 55: 147–179

Furlan S, Clauer N, Chaudhuri S, Sommer F (1996) K transfer during burial diagenesis in the Mahakam Delta basin (Kalimantan, Indonesia). Clays Clay Miner 44: 157–169

Glasmann JR, Larter S, Briedis NA, Lundegard PD (1989) Shale diagenesis in the Bergen high area, North Sea. Clays Clay Miner 37: 97–112

Grathoff GH, Moore DM (1996) Illite polytype quantification using Wildfire© calculated X-ray diffraction patterns. Clays Clay Miner 44: 835–842

Guillaume M (1986) Révision stratigraphique des couches rouges de la nappe des Préalpes Médianes romandes (unpublished). PhD thesis, Univ Fribourg, Switzerland

Hames WE, Bowring SA (1994) An empirical evaluation of the argon diffusion geometry in muscovite. Earth Planet Sci Lett 124: 161–167

Hamilton PJ, Kelley S, Fallick AE (1989) K-Ar dating of illite in hydrocarbon reservoirs. Clay Miner 24: 215–231

Hassanipak AA, Wampler JM (1996) Radiogenic argon released by stepwise heating of glauconite and illite: the influence of composition and particle size. Clays Clay Miner 44: 717–726

Hess JC, Lippolt HJ (1994) Compilation of K/Ar measurements on HD-B1 standard biotite; 1994 status report. In: Odin GS (ed) Phanerozoic time scale. Bull Lias Inf IUGS Subcomm Geochronol 12: 19–23

Hunziker JC, Frey M, Clauer N, Dallmeyer RD, Friedrichsen H, Flehmig W, Hochstrasser K, Roggwiler P, Schwander H (1986) The evolution of illite to muscovite: mineralogical and isotopic data from the Glarus Alps, Switzerland. Contrib Mineral Petrol 92: 157–180

Kübler B (1984) Les indicateurs des transformations physiques et chimiques dans la diagenèse, température et calorimétrie. In: Lagache M (ed) Thérmobarométrie et barométrie géologiques. Soc Fr Mineral Cristallogr Paris: 489–596

Jaboyedoff M, Thélin P (1996) New data on the low-grade metamorphism in the Briançonnais domain of the Prealps, western Switzerland. Eur J Mineral 8: 577–592

Kirschner DL, Cosca MA, Masson H, Hunziker JC (1996) Staircase $^{40}Ar/^{39}Ar$ spectra of fine-grained white mica; timing and duration of deformation and empirical constraints on argon diffusion. Geology 24: 747–750

Lanson B, Besson G (1992) Characterization of the end of smectite to illite transformation: decomposition of X-Ray patterns. Clays Clay Miner 40: 40–52

Lanson B, Meunier A (1995) La transformation des interstratifiés ordonnés ($S >= 1$) illite-smectite en illite dans les series diagenetiques: etat des connaissances et perspectives. Bull Centres Rech Explor Prod 19: 149–165

Markley JM, Teyssier C, Cosca MA, Caby R, Hunziker JC, Sartori M (1998) Alpine deformation and $^{40}Ar/^{39}Ar$ geochronology of synkinematic white micas in the Siviez–Mischabel Nappe, western Penninic Alps, Switzerland. Tectonics 17: 407–425

Matthews JC, Velde B, Johansen H (1994) Significance of K-Ar ages of authigenic illitic clay minerals in sandstones and shales from the North Sea. Clay Miner 29: 379–389

Meunier A, Velde B (1989) Solid solutions in I/S mixed-layer minerals and illite. Am Mineral 74: 1106–1112

Moore DM, Reynolds RC (1997) X-ray diffraction and the identification and analysis of clay minerals. Oxford Univ Press, Oxford

Mosar J (1988) Metamorphisme transporté dans les Préalpes. Schweiz Mineral Petrogr Mitt 68: 77–94

Mosar J (1989) Déformation interne dans les Préalpes Médianes (Suisse). Eclogae Geol Helv 82: 517–540

Mosar J (1991) Géologie structurale dans les Préalpes Médianes (Suisse). Eclogae Geol Helv 84: 689–725

Mossmann JR, Clauer N, Liewig N (1992) Dating thermal anomalies in sedimentary basins; the diagenetic history of clay minerals in the Triassic sandstones of the Paris Basin, France. Clay Miner 27: 211–226

Onstott TC, Mueller C, Vrolijk PJ, Pevear DR (1997) Laser $^{40}Ar/^{39}Ar$ microprobe analyses of fine-grained illite. Geochim Cosmochim Acta 61: 3851–3861

Peacor DR (1992) Diagenesis and low-grade metamorphism of shales and slates. In: Buseck PR (ed) Minerals and reactions at the atomic scale: transmission electron microscopy. (Reviews in Mineralogy 27) Mineral Soc Am, Washington, DC, pp 335–376

Perry EAJr (1974) Diagenesis and the K-Ar dating of shales and clay minerals. Geol Soc Am Bull 85: 827–830

Pevear DR (1992) Illite age analysis, a new tool for basin thermal history analysis. In: Kharaka YK, Maest AS (eds) Water rock interaction. A.A. Balkema, Rotterdam, pp 1251–1254

Pevear DR, Schuette JF (1993) Inverting the Newmod© X-ray diffraction forward model for clay minerals using genetic algorithms. In: Reynolds RC, Walker JR (eds) Computer applications to X-ray powder diffraction analysis of clay minerals. CMS workshop lectures, Clay Mineral Soc, pp 20–41

Pollastro RD (1993) Considerations and applications of the illite/smectite geothermometer in hydrocarbon-bearing rocks of Miocene to Mississippian age. Clays Clay Miner 41: 119–133

Reuter A (1987) Implications of K-Ar ages of whole-rock and grain-size fractions of metapelites and intercalated metatuffs within an anchizonal terrane. Contrib Mineral Petrol 97: 105–115

Reuter A, Dallmeyer RD (1989) K-Ar dating and $^{40}Ar/^{39}Ar$ dating of cleavage formed during very low grade metamorphism: a review. In: Daly JS, Cliff RA, Yardley BWD (eds) Evolution of metamorphic belts. Geol Soc Spec Publ, pp 161–171

Reynolds RCJr (1985) NEWMOD© a computer program for the calculation of one-dimensional X-Ray diffraction patterns of mixed-layered clays. Hanover, New Hampshire

Reynolds RCJr, Reynolds RCJr II (1996) NEWMOD© a computer program for the calculation of one-dimensional diffraction patterns of mixed-layered clays, Hanover, New Hampshire

Samson SD, Alexander ECJ (1987) Calibration of the interlaboratory $^{40}Ar/^{39}Ar$ dating standard, MMhb-1. Chem Geol 66: 27–34

Sartori M (1990) L'unité du Barrhorn. Mem Geol Lausanne 6

Shau YH, Peacor DR, Essene EJ (1990) Corrensite and mixed-layer chlorite/corrensite in metabasalt from northern Taiwan; TEM/AEM, EMPA, XRD, and optical studies. Contrib Mineral Petrol 105: 123–142

Srodon J, Elsass F, McHardy WJ, Morgan DJ (1992) Chemistry of illite-smectite inferred from TEM measurements of fundamental particles. Clay Miner 27: 137–158

Stampfli GM, Mosar J, Marquer D, Marchant R, Baudin Th, Borel G (1998) Subduction and obduction processes in the Swiss Alps. Tectonophysics 296: 159–204

Thomas AR, Dahl WM, Hall CM (1993) $^{40}Ar/^{39}Ar$ analysis of authigenic muscovite, timing of stylolitization, and implications for pressure solution mechanisms: Jurassic Norphlet formation, offshore Alabama. Clays Clay Miner 41: 269–279

Trümpy R (1980) An outline of the geology of Switzerland. Wepf and Co, Basel

Velde B, Renac C (1996) Smectite to illite conversion and K-Ar ages. Clay Miner 31: 25–32

Weaver CE, et al (1984) Shale-slate metamorphism in southern Appalachians. (Developments in petrology, vol 10). Elsevier, Amsterdam

Whitney G, Velde B (1993) Changes in particle morphology during illitization: an experimental study. Clays Clay Miner 41: 209–218

Wijbrans JR, McDougall I (1986) $^{40}Ar/^{39}Ar$ dating of white micas from an Alpine high-pressure metamorphic belt on Naxos (Greece): the resetting of the argon isotopic system. Contrib Mineral Petrol 93: 187–194